PETROGRAPHY OF THE UTAH FORGE SITE AND ENVIRONS, BEAVER COUNTY, UTAH

by Clay G. Jones, Joseph N. Moore, and Stuart Simmons

Energy & Geoscience Institute, University of Utah, Salt Lake City, Utah

Miscellaneous Publication 169-K
Utah Geological Survey
a division of
UTAH DEPARTMENT OF NATURAL RESOURCES

This paper is part of *Geothermal Characteristics of the Roosevelt Hot Springs System and Adjacent FORGE EGS Site, Milford, Utah*. https://doi.org/10.34191/MP-169

Bibliographic citation:

Jones, C.G., Moore, J.N., and Simmons, S., 2019, Petrography of the Utah FORGE site and environs, Beaver County, Utah, *in* Allis, R., and Moore, J.N., editors, Geothermal characteristics of the Roosevelt Hot Springs system and adjacent FORGE EGS site, Milford, Utah: Utah Geological Survey Miscellaneous Publication 169-K, 23 p., 2 appendices, https://doi.org/10.34191/MP-169-K.

PETROGRAPHY OF THE UTAH FORGE SITE AND ENVIRONS, BEAVER COUNTY, UTAH

by Clay G. Jones, Joseph N. Moore, and Stuart Simmons

ABSTRACT

In this paper we focus on the characterization of core and cuttings recovered from geothermal wells 58-32 and Acord-1 using petrographic, X-ray diffraction (XRD) and scanning electron microscope (SEM) techniques. Well 58-32 was drilled to 7536 ft measured depth in 2017 as part of the Utah Frontier Observatory for Research in Geothermal Energy (FORGE) project. Acord-1 is a 12,650-ft-deep exploratory geothermal well drilled in 1979 in the central part of the Milford Valley. For comparison, samples have also been analyzed from outcrops in the Mineral Mountains and from geothermal wells 9-1, 52-21 and 14-2 drilled within and adjacent to the Roosevelt Hot Springs geothermal field.

Well 58-32 primarily penetrated two rock types: alluvium in the upper part of the well (0–3176 ft) and coarse-grained plutonic rocks in the lower portion (3195–7536 ft). Separating these two lithologies is a thin, sheared rhyolite (3176–3195 ft). Acord-1 penetrated a thick sequence of basin fill consisting of lacustrine sediments, evaporite deposits, volcaniclastic deposits, ash-flow tuffs, tuffaceous sediments and andesite lava flows before reaching the plutonic rocks of the Mineral Mountains Batholith at ~10,175 ft.

Formation Microscanner Image (FMI) logs of well 58-32, petrographic analyses and the results of a 3-D seismic survey provide no evidence that the sediments and volcanic rocks of the basin fill have undergone significant deformation or contact metamorphism. In contrast, the underlying plutonic rocks encountered in Acord-1 and well 58-32 are intensely sheared and brecciated. The contact between the basin fill and plutonic rocks dips at approximately 25° to the west. Westward-dipping, shallow bedding planes in the alluvium of well 58-32 are also observed in the FMI log. These observations suggest the basin fill was deposited on an exposed and rotated range front fault as discussed by Bartley et al. (2018).

In well 58-32, samples from >6500 ft, where measured temperatures exceed 347°F (175°C), are within the Enhanced Geothermal System (EGS) reservoir. At these depths the plutonic rocks consist dominantly of granite and quartz monzonite with minor granodiorite, quartz monzodiorite and fine-grained banded diorite. Except for relatively rare banded diorite, the plutonic rocks are composed of 90–97 wt% quartz, K-feldspar and plagioclase, with minor biotite, hornblende, titanite, apatite, magnetite/ilmenite and zircon. Alteration is weak and shows no clear relationship to temperature. The most common secondary minerals are the clay minerals, with illite > chlorite> interlayered illite/smectite > smectite and carbonates. Other secondary minerals include anhydrite, hematite, epidote, quartz and plagioclase.

INTRODUCTION

The Frontier Observatory for Research in Geothermal Energy (FORGE) has been envisioned by the U.S. Department of Energy as a dedicated site where scientists and engineers will be able to develop, test, and accelerate breakthroughs in Enhanced Geothermal System (EGS) technologies and techniques. In this paper we present petrographic, X-ray diffraction (XRD), and scanning electron microscope (SEM) analyses of well cuttings, core, and outcrop samples from the Utah FORGE site and wells drilled in the surrounding area (Figure 1), with emphasis on the plutonic rocks that comprise the EGS reservoir.

METHODS

Petrographic Analysis

Three hundred and fifty-four thin sections were analyzed to document rock type, primary and secondary mineral assemblages, evidence of brittle and ductile deformation, and the paragenetic relationships of open-space filling minerals.

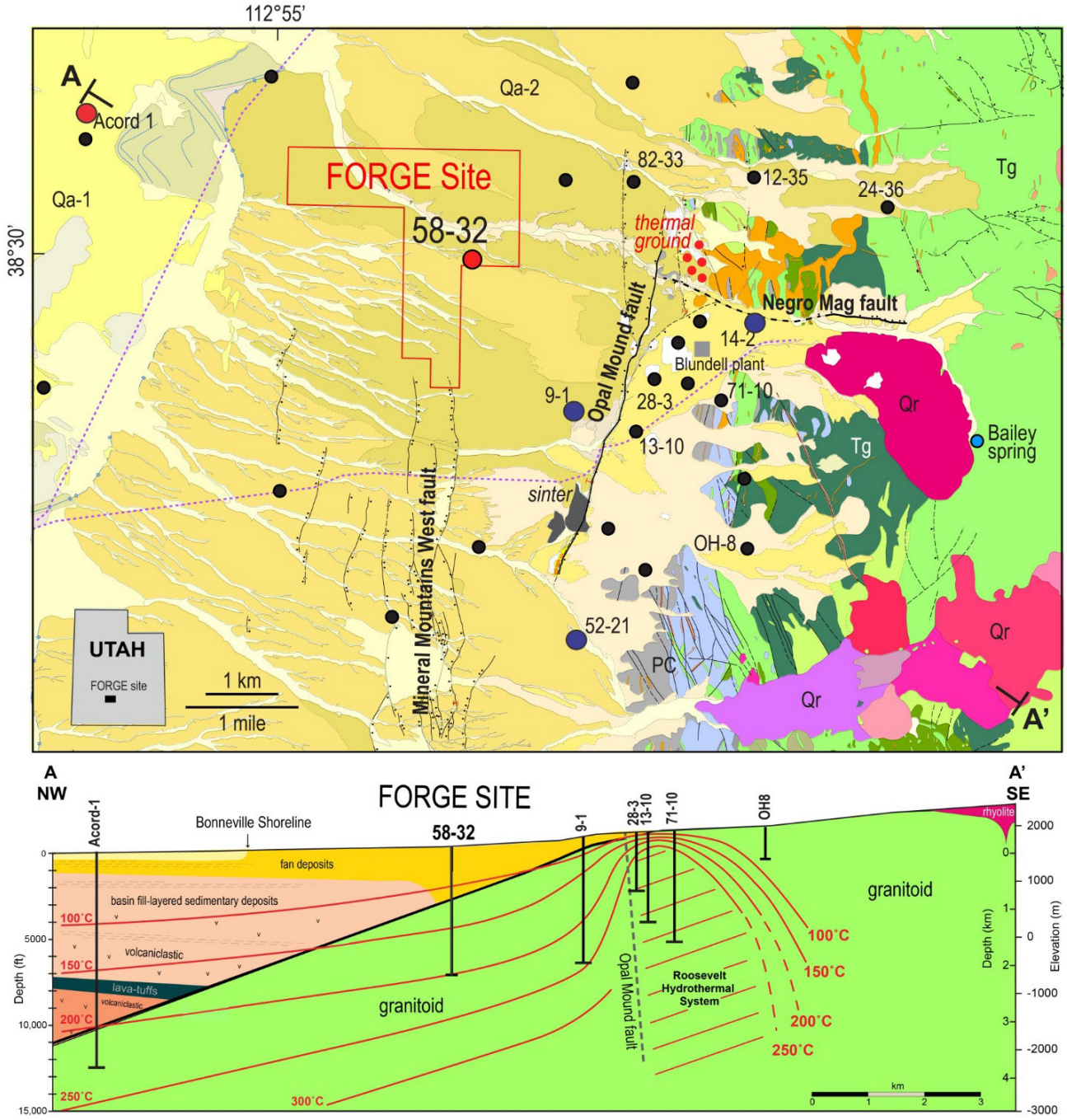

Figure 1. *Geologic map and cross section (no vertical exaggeration) of the Utah FORGE site and environs (modified from Kirby et al., 2018). In the cross section the intrusive lithologies of the Mineral Mountains Batholith have been combined and are shown as simply "granitoid." Wells from which samples were selected for this study include Acord-1 and 58-32 (large red circles), as well as 9-1, 52-21 and 14-2 (large dark-blue circles). Other wells are shown as black circles. All outcrop samples analyzed come from within the bounds of this map.*

X-Ray Diffraction (XRD)

Two hundred and forty-seven whole-rock and clay-sized (< 5 µm size fraction) XRD analyses were performed at the Energy & Geoscience Institute on a Bruker D-8 Advance XRD system. The following operating parameters were used: Cu-Kα radiation at 40 kV and 40 mA; 0.02°2θ step size; and a scan rate of 0.4 to 0.6 seconds per step. The clay-size fraction was examined from 2 to 45°2θ, and the whole-rock samples from 4 to 65°2θ. Phase quantification of whole-rock samples using the Rietveld method were performed using TOPAS software. Clay mineral species were identified by comparing the air-dried and glycolated clay-size fraction diffractograms using the techniques of Moore and Reynolds (1997). Results from all XRD analyses are provided in Appendix A.

Scanning Electron Microscopy (SEM)

SEM analyses were conducted on 11 polished thin sections of the two cored intervals of 58-32, as well as polished thin section billets from a handful of select cuttings samples from 58-32. SEM analyses were performed at the Energy & Geoscience Institute using a JEOL IT300 SEM.

DESCRIPTIONS OF THE LITHOLOGIES ENCOUNERED IN UTAH FORGE WELL 58-32

Analysis of core and cuttings from FORGE well 58-32 show that alluvium was penetrated in the upper part of the well (0–3176 ft), and coarse-grained plutonic rocks were encountered in the lower part (3195–7536 ft). Separating these two lithologies is a thin sheared and brecciated porphyritic rhyolite (3176–3195 ft) (Figure 2).

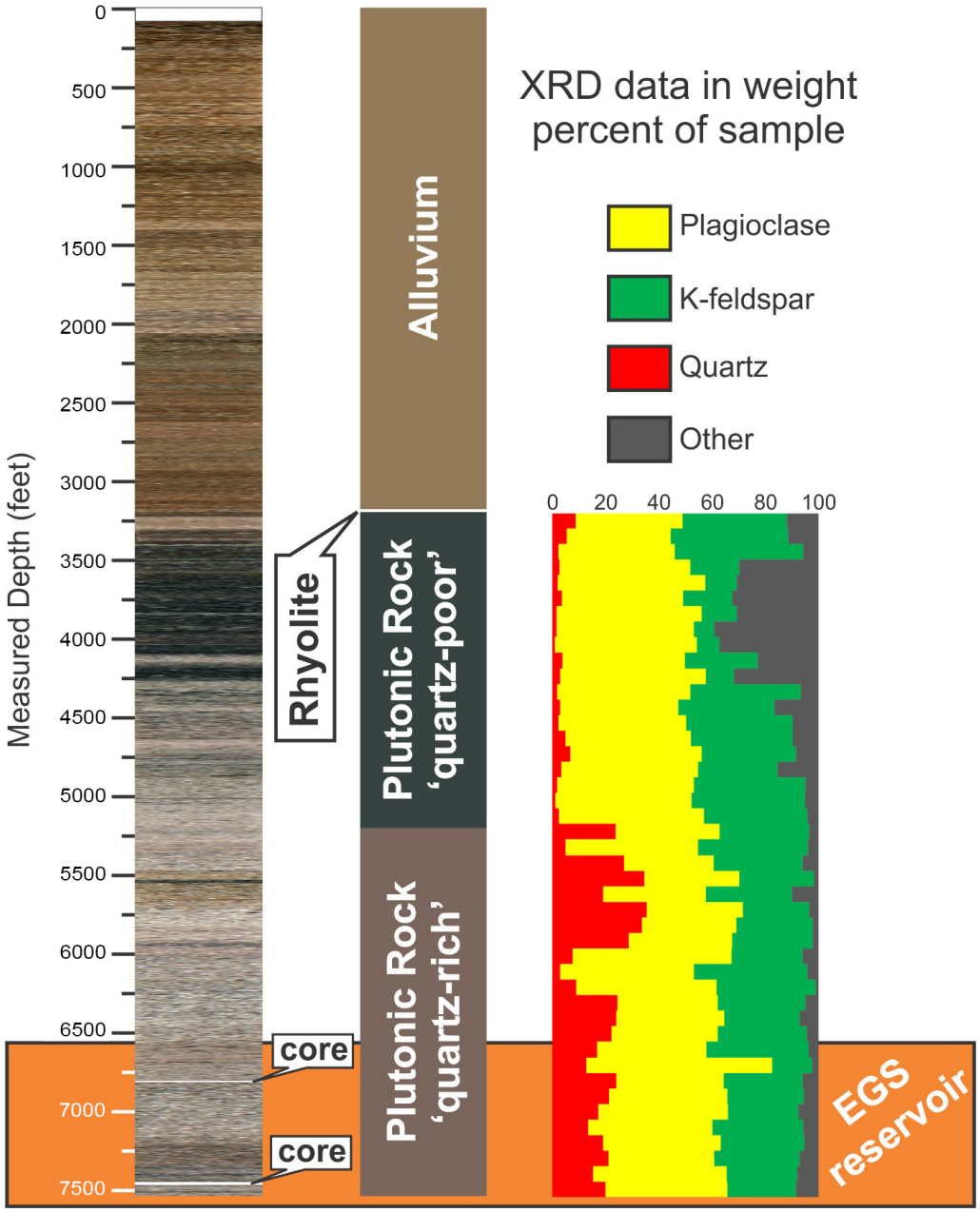

Figure 2. *At left is a lithologic column constructed from compressed images of the well cuttings from 58-32, with a simplified lithologic column at center. At right is XRD data from the plutonic rock analyzed at 100-ft intervals. Two cores were taken at the depths indicated. The proposed EGS reservoir (shown in orange) is at depths greater than 6528 ft where temperatures in excess of 347°F (175°C) have been measured.*

Alluvium (0–3176 ft)

The alluvial deposits in the upper part of the well (0–3176 ft) were clearly imaged in the FMI log as poorly sorted sediments containing boulders up to several feet in diameter with minor finer-grained deposits. The FMI log also shows bedding planes that dip predominantly westward, mimicking the topography of the Milford basin and the top of the underlying plutonic rocks. These are poorly-lithified sediments that have not experienced contact metamorphism, nor have they been indurated by hydrothermal fluids. Disaggregation of the sediments during drilling and washing of the cuttings removed much of the smaller than sand-size fraction, therefore the XRD data are skewed to reflect the composition of the clasts and larger mineral grains. The clasts consist of plutonic rock similar in both composition and texture to those outcropping in the Mineral Mountains to the east of the Roosevelt geothermal field and the plutonic rock encountered at deeper levels of well 58-32 ("quartz-rich" plutonic rocks of Figure 2). Secondary minerals compose 1 to 5 wt% of the cuttings and include illite, hematite, and smectite. No open-space filling mineralization was observed binding clasts together (i.e., cement). Hematite (up to 2 wt%) in the alluvium cuttings gives them a reddish-brown color compared to the cuttings of the plutonic rock below (Figure 2).

Rhyolite (3176–3195 ft)

An approximately 19-ft-thick zone of sheared and brecciated porphyritic rhyolite occupies a short vertical interval (3176–3195 ft) at the unconformity between the alluvium above and the plutonic rocks below. The rhyolite was initially identified as an area of interest in the FMI log, due to its distinct resistivity texture (Figure 3). Cuttings from this interval contain resorbed quartz (Figure 4) and less abundant alkali feldspar phenocrysts in a fine-grained equigranular groundmass composed of intergrown K-feldspar and quartz with minor spherulitic devitrification textures. The devitrification textures suggest that this lithology was originally glassy and cooled slowly, allowing these microstructures to form. It is not clear if this unit represents an extrusive rhyolite flow or a shallow intrusion.

Evidence of shearing and brecciation of the rhyolite includes cataclasites, silica-cemented breccias, and veining. The cataclasites contain vein fragments and are cut by veins (Figure 4). Paragenetic relationships suggest that there have been at least three episodes of brittle deformation and open-space mineralization (Figure 4): 1) early botryoidal chalcedony (subsequently recrystallized to quartz) followed by multiple generations of quartz ranging from fine-grained to coarse-grained and euhedral in texture; 2) an episode of feldspar dissolution and kaolinite precipitation in the resulting open space; and 3) late veins filled by calcite ± hematite. Similar evidence of high paleo-permeability was not observed in the alluvium above, nor the plutonic rock below. There was no evidence of modern permeability observed during drilling (i.e., no lost circulation).

The observed paragenetic relationships within the rhyolite documents changes in physical and chemical conditions with time. The transition from chalcedony to quartz may indicate an increase in temperature. In geothermal systems, chalcedony is the stable polymorph at temperatures less than ~180°C, and quartz is stable at higher temperatures (Fournier, 1985). Alternatively, the paragenetic relationship of chalcedony before quartz without a hiatus in deposition has been attributed to boiling resulting in supersaturation of silica and precipitation of chalcedony below its typical temperature stability field (e.g., Moore et al., 2008). Localized boiling could occur during a pressure drop caused by fault rupture. Measured temperatures at this depth are ~100°C, well below the stability of quartz, suggesting that the observed silica deposition occurred earlier under a different temperature regime. Following silica deposition was an episode of K-feldspar dissolution and kaolinite precipitation. It is not clear if this records an episode of extensive weathering or interaction of the rhyolite with an acidic hydrothermal fluid. The last open-space minerals to precipitate in the rhyolite are calcite and hematite. The co-precipitation of calcite and hematite is likely the result of downward percolation and heating of oxidized fluids.

Plutonic Rocks (3195–7536 ft)

The FORGE EGS reservoir is hosted by the plutonic rocks of the Mineral Mountains Batholith. The batholith is thought to have been emplaced in two pulses: 1) 25 ± 4 Ma (Aleinikoff et al., 1986); and 2) 18.2–17.5 Ma (Coleman, 1991; Coleman and Walker, 1992). These two periods of plutonic emplacement have been interpreted as the result of coeval intrusion and mixing of mafic and felsic magmas (Coleman, 1991; Coleman and Walker, 1992). Later events include coeval rhyolite and basalt dikes at ~11 Ma (Coleman and Walker, 1994) and the eruption of rhyolite domes along the crest of the range at 0.8–0.5 Ma (Lipman et al., 1978).

Within the plutonic rocks intersected by well 58-32, the most striking shift in bulk mineralogy was observed between 5100–5110 and 5200–5210 ft, with relatively "quartz-poor" plutonic rock above and "quartz-rich" plutonic rock below (Figures 2 and 5). The quartz-poor rocks (Figure 6) are finer grained, generally darker in color due to higher a proportion of ferromagnesian

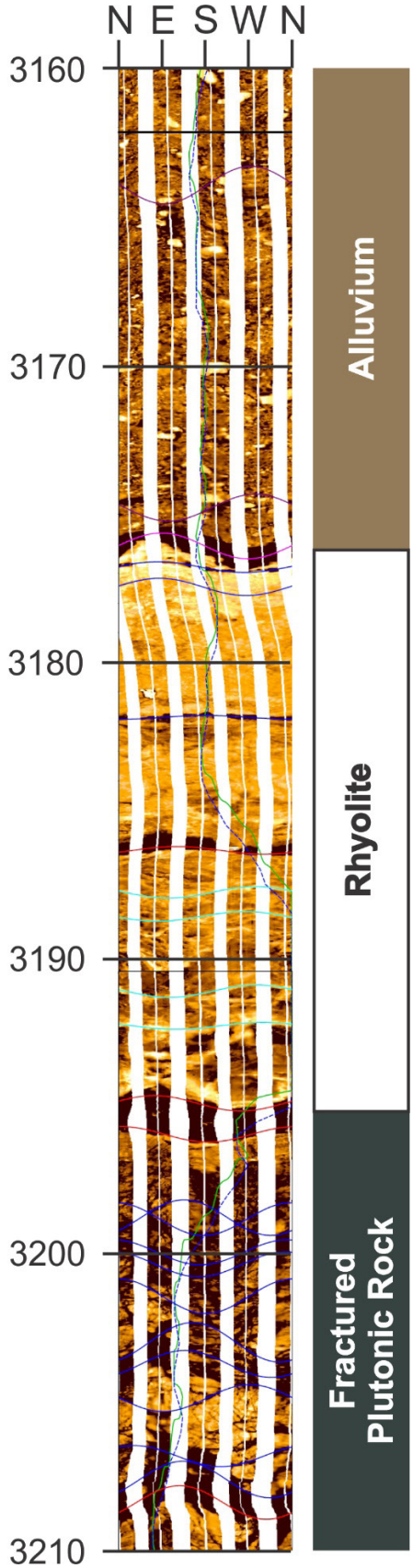

Figure 3. *A 50-ft interval of the FMI log run in well 58-32 that shows the transition from alluvium to plutonic rock. Rhyolite separates these two lithologies (3176–3195 ft). The sinusoidal lines on the FMI image are interpreted fractures and most are concentrated in the plutonic rock. The FMI image is a 2-D representation of the cylindrical borehole from north (0°) on the left, to south (180°) in the middle, back to north (360°) on the right. In this FMI log lighter areas are more resistive than darker areas.*

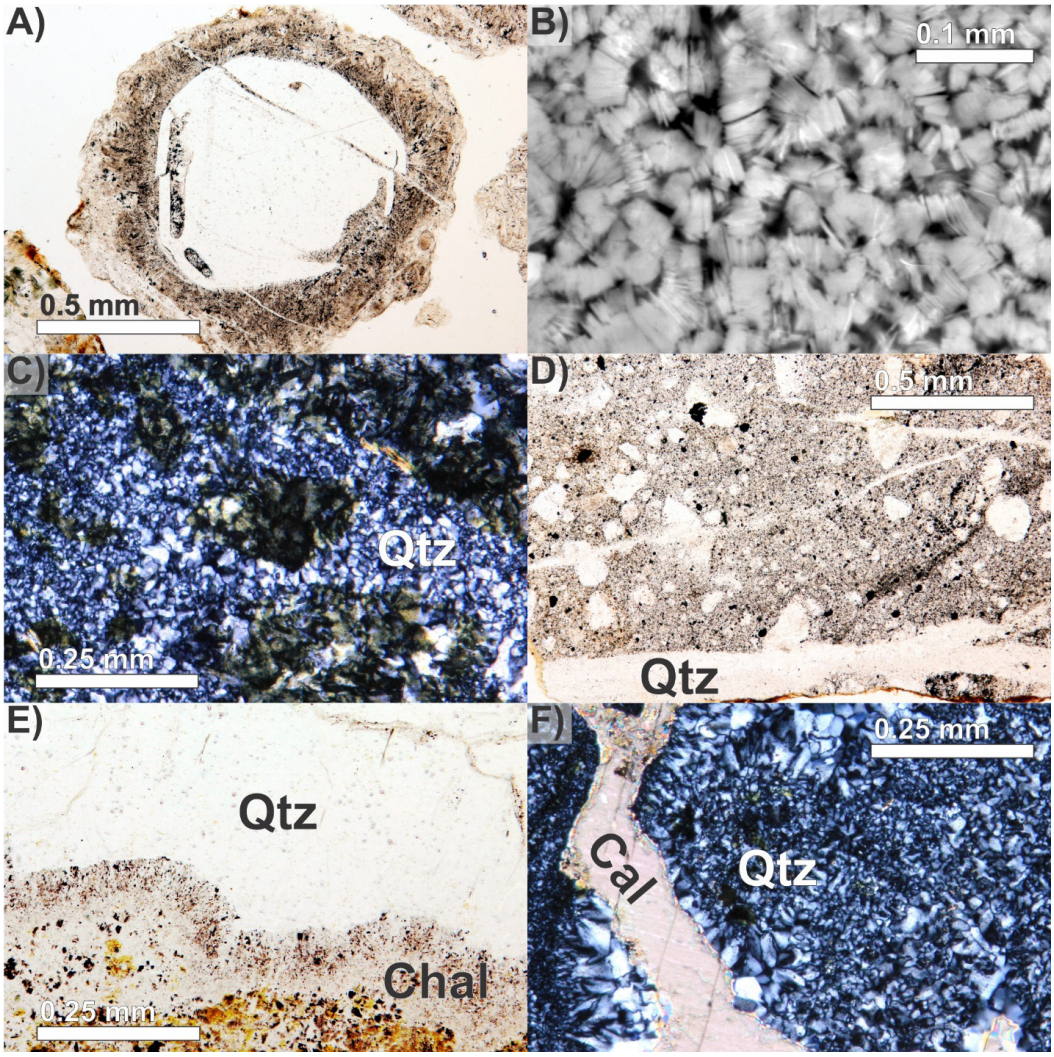

Figure 4. *Images of the rhyolite.* ***(A)*** *Plane-polarized light (PPL) photomicrograph of a partially resorbed quartz phenocryst.* ***(B)*** *Backscatter SEM image of kaolinite filling open space.* ***(C)*** *Crossed-polarized light (XPL) images of quartz- (Qtz) cemented breccia. The K-feldspar in the wall rock has been stained.* ***(D)*** *PPL photomicrograph of cataclasite cut by later quartz veins.* ***(E)*** *PPL photomicrograph of a vein filled by botryoidal chalcedony (Chal) before euhedral quartz. K-feldspar stained yellow in the wall rock.* ***(F)*** *XPL photomicrograph of a late calcite (Cal) vein cutting an earlier quartz vein.*

minerals (biotite + hornblende ± clinopyroxene), and can be compositionally banded. The quartz-rich lithologies (Figure 7) are coarser grained, contain fewer ferromagnesian minerals, and may exhibit a subtle foliation. Small-scale changes in texture and mineralogy are common. In both cored intervals of 58-32 changes in mineralogy and/or rock type were observed (Figure 8). Similar compositional variations were observed in outcrops of the Mineral Mountains.

Core and cutting samples at 6600 ft or deeper in 58-32 are within the FORGE EGS reservoir where temperatures exceed 347°F (175°C) and are composed primarily of granite and quartz monzonite with less-abundant quartz monzodiorite, granodiorite, and diorite (Figure 8). Except for the banded diorite in the lower core, the EGS reservoir rocks are composed of 90–97 wt% quartz, K-feldspar, and plagioclase, with the remainder of the primary minerals consisting of (in decreasing order of abundance) biotite, hornblende, titanite, apatite, and zircon. In contrast, the diorite in the cored section of well 58-32 contains 58–67 wt% quartz, K-feldspar and plagioclase; and 30–35 wt% biotite and hornblende.

To document the textures of the plutonic rocks within the EGS reservoir, SEM backscatter photomosaic images were made of 1.5-inch-diameter core plugs taken at horizontal and vertical orientations relative to the core (Figure 9). In these backscatter SEM images, minerals consisting of elements having higher average atomic numbers are relatively lighter gray in color. Lithologies 1, 2, and 4 in Figure 9 are coarse-grained compared to the banded diorite (lithology 3). The coarse-grained rocks in the upper core (lithologies 1 and 2) are equigranular with a subtle foliation, whereas the coarse-grained rock in the lower core (lithology 4) has a slightly porphyritic texture with large, rounded K-feldspar phenocrysts with no apparent foliation.

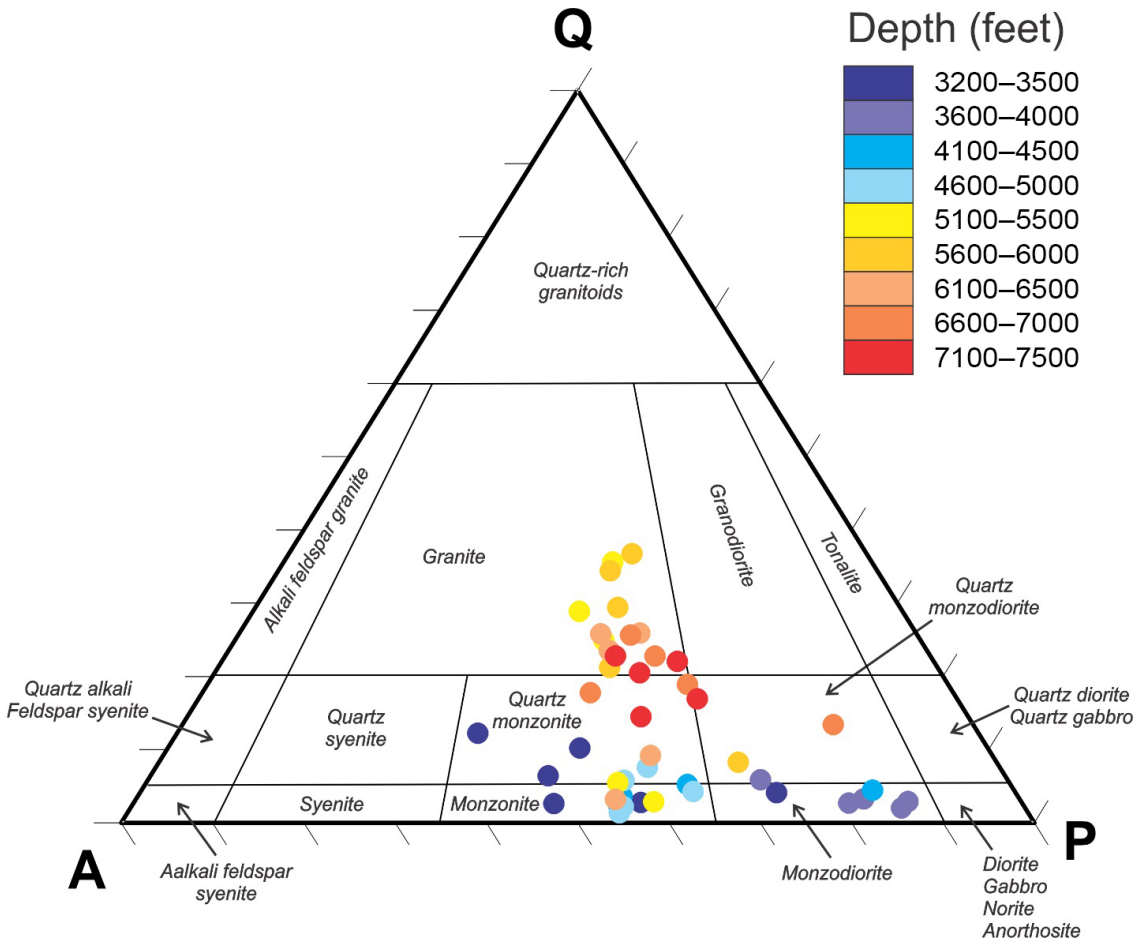

Figure 5. *XRD data from the plutonic rocks in well 58-32. The data have been normalized to 100 weight percent quartz (Q), K-feldspar (A), and plagioclase (P) and plotted on the IUGS classification diagram (Le Maitre et al., 1989). The samples have been color coded by depth. Cuttings from within the EGS reservoir at depths ≥ 6600 ft where temperature exceed 347°F (175°C) are shown in red and darkest orange and plot primarily in the granite and quartz monzonite fields.*

Alteration mineralogy in plutonic rocks

The abundance of alteration minerals is generally low in the plutonic rock from well 58-32 and decreases with depth (Figure 10), suggesting decreasing permeability. Three intervals in the upper basement that consisted of sheared/brecciated and veined rock contain higher abundances of alteration minerals; however, the vast majority of cutting samples contain less than 7 wt%, and within the EGS reservoir secondary minerals make up only a few wt% of the samples on average.

Clay minerals are the most common secondary minerals observed in 58-32 (Figure 10) and include smectite, interlayered chlorite/smectite, chlorite, illite, and kaolinite. Within the plutonic rocks, clay minerals replace primary minerals; plagioclase is dominantly altered to illite with less abundant smectite and chlorite (Figure 11A), and ferromagnesian minerals are dominantly altered to chlorite with less abundant interlayered chlorite/smectite and smectite. Other secondary minerals include carbonates (calcite > siderite > dolomite), epidote, quartz, hematite and anhydrite. Alteration of plagioclase to epidote (Figure 11B) was regularly observed; however, epidote abundances are low (< 1 wt% by XRD). Calcite and anhydrite also sporadically replace plagioclase in low abundances.

Open-space filling minerals in plutonic rocks

Open-space minerals in the plutonic rocks of well 58-32 are sporadically observed in low abundances (Table 1) filling veins and open space in sheared/brecciated rock. Carbonates are the most commonly observed open-space filling minerals, with calcite being the most abundant and widely distributed. Siderite and dolomite (± hematite) are locally concentrated in a few samples towards the top of the basement in sheared/brecciated rocks (Figure 11C) in abundances ranging from 3 to 6 wt%. Anhydrite and/or hematite may be found within carbonate veins.

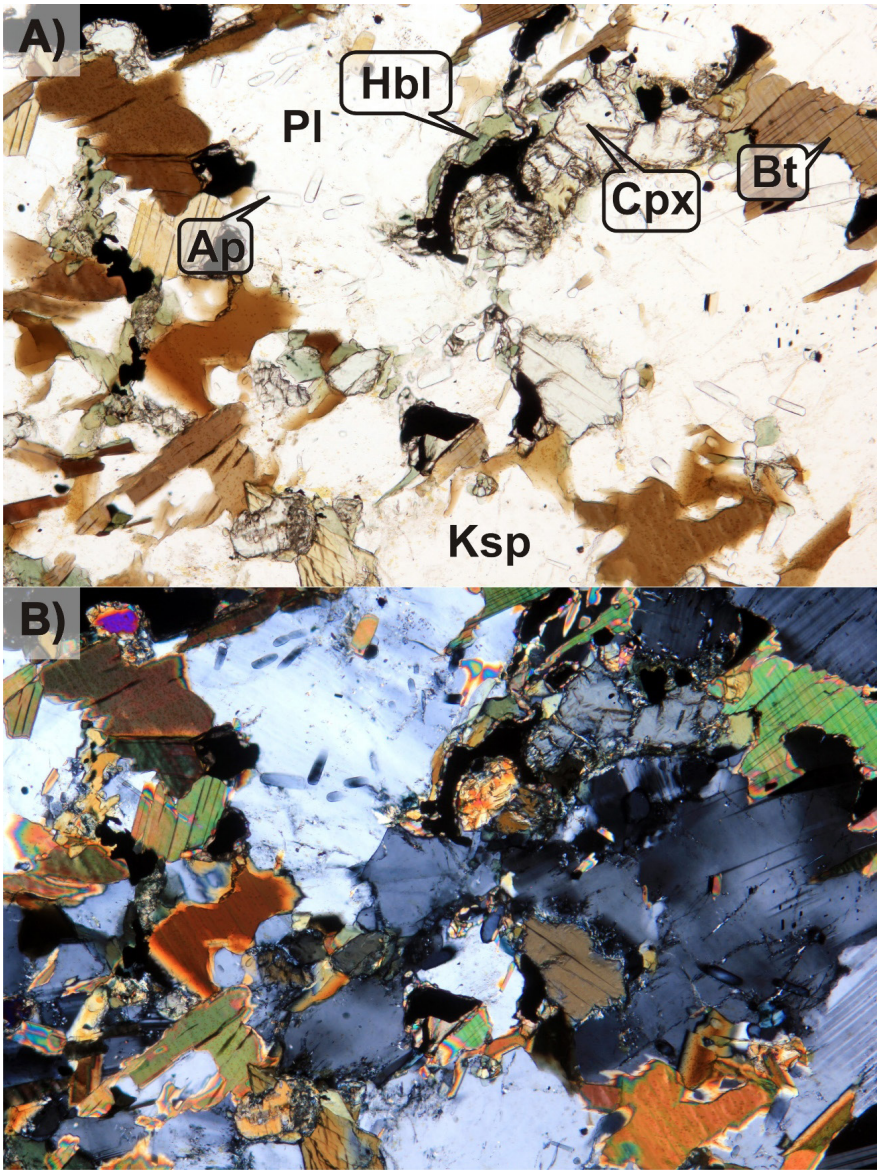

Figure 6. *Representative photomicrograph of a quartz-poor plutonic rock (monzodiorite) from 3700–3710 ft in well 58-32.* ***(A)*** *Plane-polarized light.* ***(B)*** *Crossed-polarized light. Field of view = 1.6 mm. Ap = apatite, Bt = biotite, Cpx = clinopyroxene, Hbl = hornblende, Ksp = K-feldspar, and Pl = plagioclase.*

Quartz, plagioclase, epidote, and chlorite locally fill open space; however, modern temperatures are below their respective stability ranges, suggesting that they formed during an earlier alteration event and are therefore older than the carbonate and/or anhydrite veins, which may be stable under modern in situ conditions.

Only a few mineralized fractures were observed in the approximately 22 ft of core recovered from 58-32. The upper core (6800–6810.25 ft) contained two steeply dipping mineralized fractures: one epidote + quartz lined, and partially sealed; the other filled by epidote. The lower core (7440–7452.15 ft) contained several mineralized fractures. Within the diorite there are multiple thin fractures sealed by plagioclase and epidote that cut across compositional banding. An epidote-filled fracture also cuts the lower granitic lithology and abruptly terminates within the diorite. Several other steeply dipping fractures in the core are likely to have been induced as they do not contain any secondary mineralization.

Microstructures in plutonic rocks

Microstructures within the plutonic rocks of 58-32 (Figure 12) provide a record of both plastic and brittle deformation. Table 1 shows microstructures observed during thin section petrographic analysis of the cuttings of 58-32 at 100 ft intervals. Observed microstructures that record plastic deformation within the EGS reservoir include mylonites, deformation twins, kink bands,

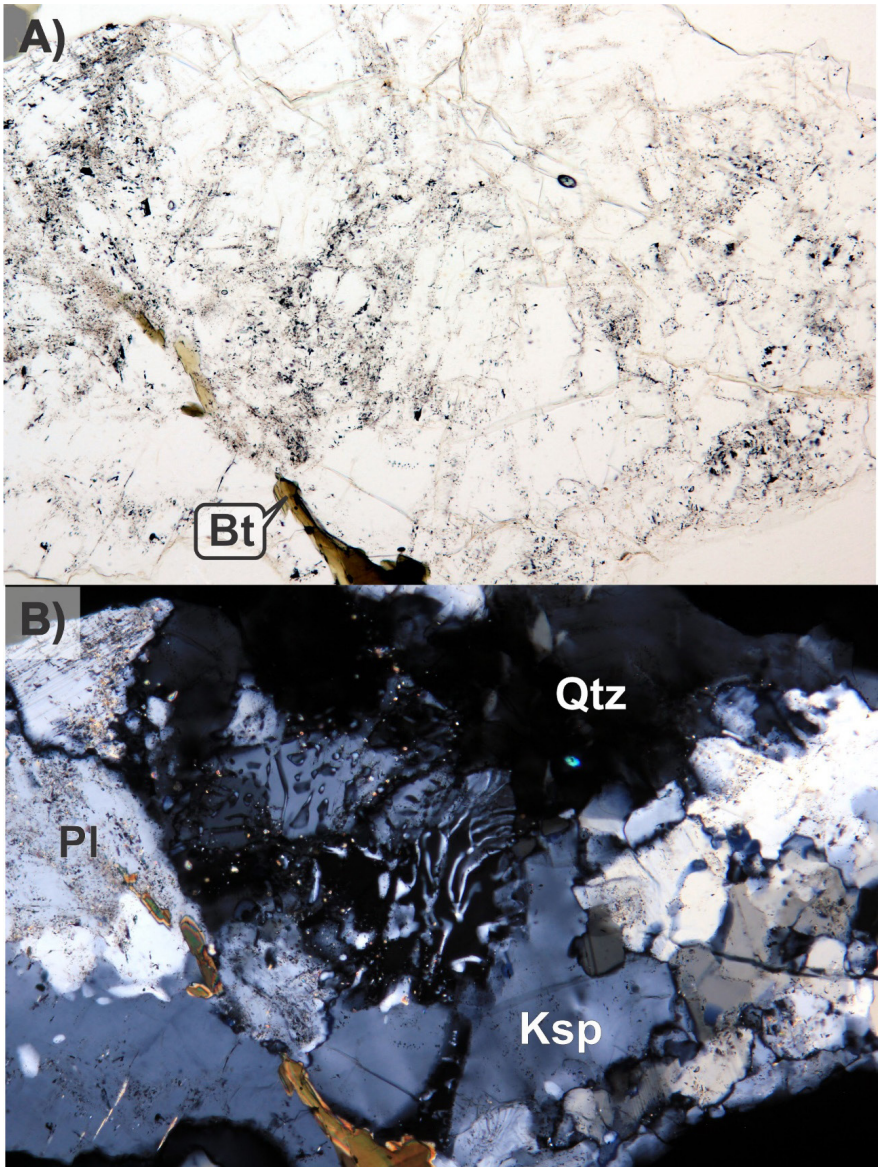

Figure 7. *Representative photomicrograph of a quartz-rich plutonic rock (granite) within the proposed EGS reservoir at 7200–7210 ft in 58-32. Myrmekite texture (Ksp replaced by worm-like Qtz in Pl) can be seen at center.* ***(A)*** *Plane-polarized light.* ***(B)*** *Crossed-polarized light. Field of view = 1.6 mm. Bt = biotite, Ksp = K-feldspar, Pl = plagioclase, and Qtz = quartz.*

deformation lamellae, dynamic recrystallization, transformation twinning, and undulatory extinction. Brittle deformation is recorded by cataclasite, shearing/brecciation, and veining. The proportion of cuttings in any given sample that display textures compatible with mylonite and/or cataclasite is generally minor and is interpreted to be the result of sampling relatively thin zones of deformation between larger blocks of more coherent plutonic rock.

Perthite (Figure 12A) and myrmekite (Figure 7) are pervasive within the EGS reservoir and the formation of both results in a net volume reduction. Perthite, the exsolution of plagioclase from alkali feldspar, leaves host grains with a turbid appearance due to the formation of micropores (Walker et al., 1995). The formation of myrmekite also results in a net volume loss (Simpson and Wintsch, 1989), but porosity within these domains is not as apparent in thin section.

Microstructures observed within the plutonic rocks of 58-32 record early plastic and later brittle deformation as the Mineral Mountains Batholith ascended from depth after emplacement to its current position at or near the earth's surface during Basin and Range extension. Microstructures can be pervasive and are likely to influence mechanical and physical properties of the EGS reservoir rock. Microstructures may locally influence the mechanical and physical properties of the rock, especially those that result in preferred mineral orientations (i.e., mylonites, dynamic recrystallization), reduced rock strength (i.e., cataclasite, brecciation), and/or increased porosity (i.e., perthite and myrmekite).

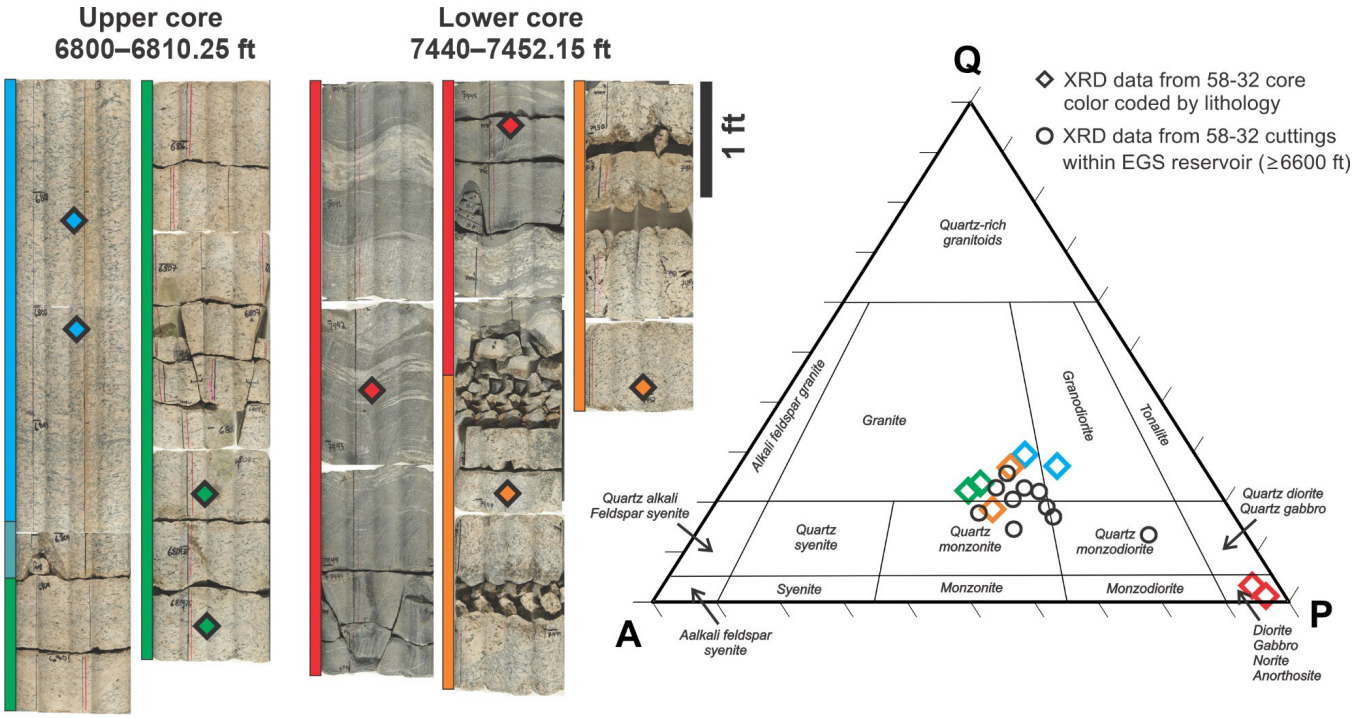

Figure 8. *Images on the left are of the two cores retrieved from well 58-32 at the depths indicated. These images are constructed from four separate images taken 90° apart that have been stitched together to give a 2-D representation of the entire cylindrical core. Colored bars next to the core indicate the four texturally distinct zones, with a subtle transition zone over less than 1 ft in the upper core (blue-green color). On the right is the XRD data from core and cuttings within the EGS reservoir, normalized to 100 weight percent quartz (Q), K-feldspar (A), and plagioclase (P) and plotted on the IUGS classification diagram (Le Maitre et al., 1989). The depths from which XRD samples were taken from the core are indicated and color-coded to the symbols on the IUGS ternary diagram.*

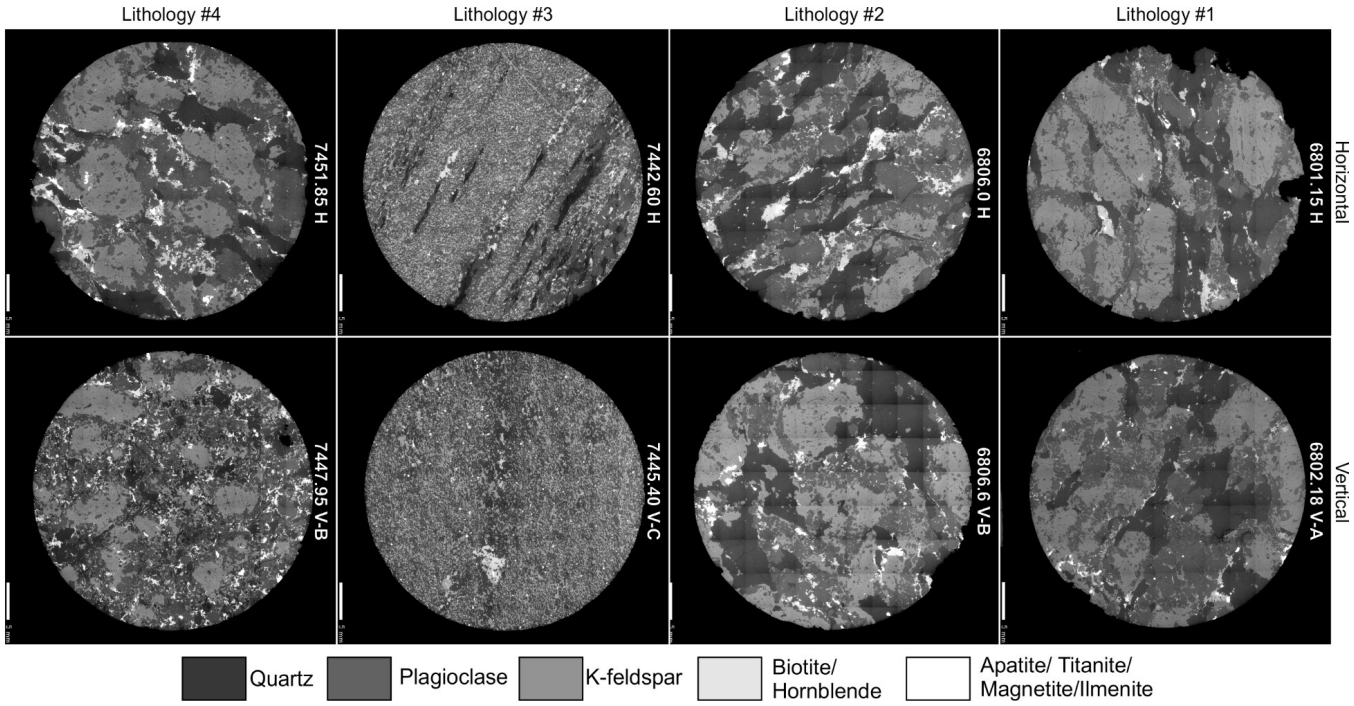

Figure 9. *Backscatter electron SEM photomosaic images of vertically and horizontally oriented 1.5-inch-diameter plugs from each of the four lithologies in the two cores from well 58-32. The approximate grayscale values by mineral are shown at right.*

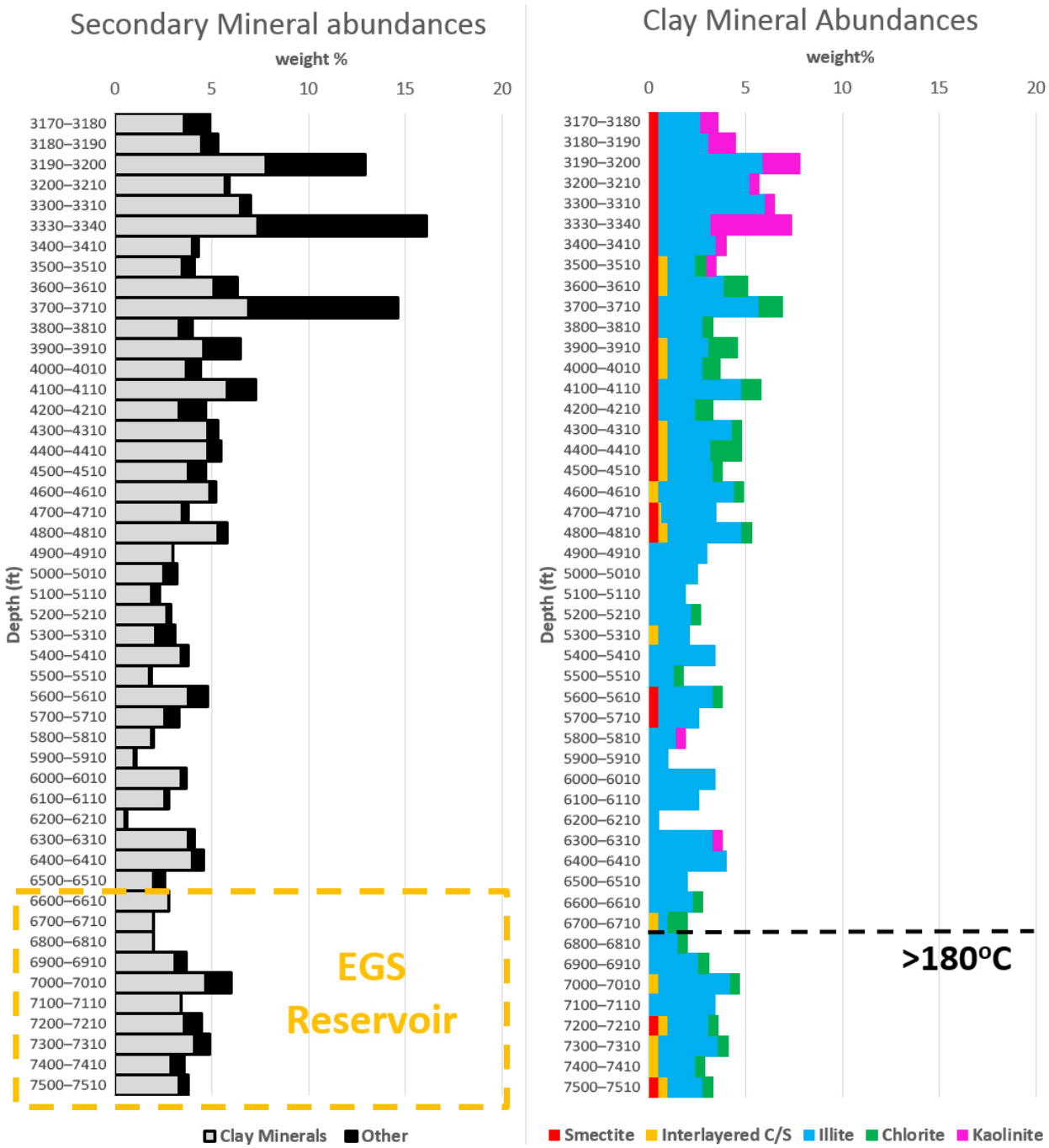

Figure 10. *Abundance of secondary minerals within the plutonic rocks of well 58-32 from XRD data. Secondary minerals observed in trace amounts during petrographic observation are shown as 0.5 wt% for visualization purposes,* possibly over-representing the total abundance of secondary minerals on this figure. *"Other" secondary minerals include: carbonates (calcite>siderite>dolomite), epidote, quartz, hematite, and anhydrite.*

DESCRIPTIONS OF THE LITHOLOGIES ENCOUNTERED IN WELL ACORD-1

Photomicrographs representative of each of the lithologies that comprise the basin fill are in Appendix B, with figure captions labeled to match the depths indicated in the subheadings below.

Basin Fill. Samples 70–100 to 10,140–10,150 ft

Acord-1 penetrated a thick sequence of basin fill consisting of lacustrine sediments, evaporite deposits, volcaniclastic deposits, ash -flow tuff and andesite lava flows before reaching the plutonic rocks of the Mineral Mountains Batholith at ~10,175 ft (Figure 13).

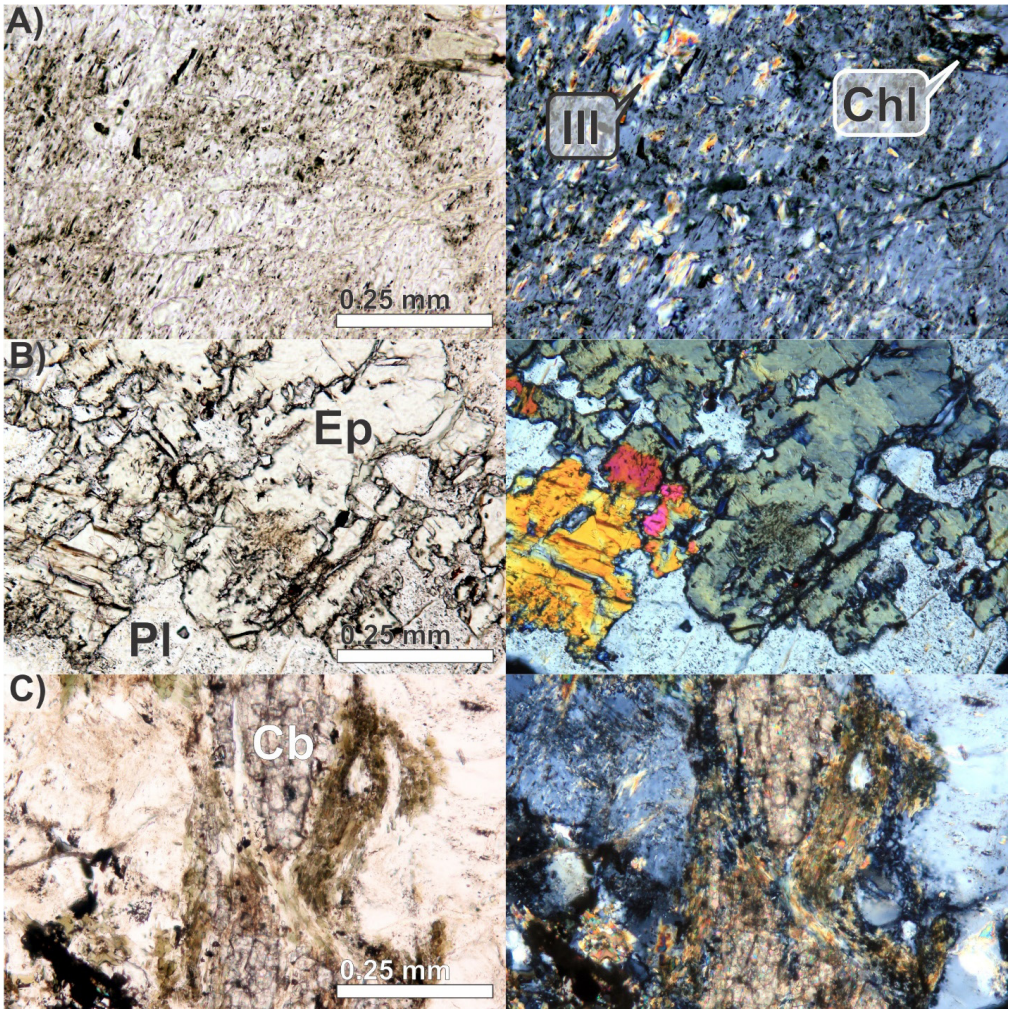

Figure 11. *Plane-polarized (left) and cross-polarized (right) photomicrographs of secondary minerals in the plutonic rock of well 58-32.* ***(A)*** *Illite (Ill) and chlorite (Chl) replacing plagioclase at 6700–6710 ft.* ***(B)*** *Epidote (Ep) replacing plagioclase (Pl) at 7400–7410 ft.* ***(C)*** *Carbonates (Cb = siderite>dolomite) filling open space and replacing sheared rock at 3700–3710 ft.*

Mixed sediments. Sample 70–100 ft

This sample contained sediments with variable grain sizes ranging from large clasts of plutonic rocks and lava flows that are at least gravel-size, to fine grained silt-size clasts predominantly composed of mineral grains. The siltstone has both clay-rich (illite and kaolinite) and fine-grained calcite matrix, and contains rare calcite-filled burrows (trace fossils). Sedimentary rip-up clasts are also incorporated into these sediments. The finer-grained fraction (siltstone and fine-grained sandstone) is generally matrix supported and the coarser-grained cuttings are cemented by calcite.

Lacustrine sediments and evaporite deposits. Samples 320–350 to 4240–4250 ft

The dominant lithology in the cuttings from this interval is siltstone, with less abundant sandstone and larger clasts of plutonic rock that are at least gravel-size. In general, the sequence becomes finer-grained towards the top of the unit. The sediments have a fine-grained matrix composed of variable proportions of clay minerals (illite and smectite ± kaolinite ± chlorite) and carbonate minerals (calcite ± dolomite). Anhydrite is intermittently observed as nodules, laths, and as thin beds with up to 35 wt% anhydrite in the sample from 3320–3350 ft. Trace fossils (burrows) are consistently observed in siltstone, whereas carbonate fossils (locally replaced by anhydrite) are more common in sandstone. Sedimentary rip-up clasts of siltstone are also a fairly consistent feature in this unit. Sandstone chips are dominantly matrix-supported, with less abundant grain-supported sandstone having calcite or anhydrite cement. The larger lithic clasts are derived primarily from plutonic rock with minor andesite lava flows and ash-flow tuffs. Rare and intermittent replacement of anhydrite by quartz and chalcedony is observed as shallow as 1340–1350 ft and minor occurrences of analcime are found from 1580–1610 to 2600–2630 ft. No evidence of brittle deformation is observed in these soft sediments.

***Table 1**. Summary of microstructures and open-space minerals observed during thin section petrography of well 58-32 cuttings samples of plutonic rock. An "X" indicates that the microstructure was observed at that depth. A "?" indicates that there are some mineral textures that may be compatible with thin mylonite zones at these depths. Mineral abbreviations used to denote which open-space minerals were observed at each depth are: Cb = carbonate; Anh = anhydrite; Ep = epidote; Chl = chlorite; and Qtz = quartz.*

Depth (ft)	Mylonite	Perthitie	Myrmekite	Cataclasite	Shearing/	Veining	Open-space filling minerals
3200–3210		X		X	X	X	Cb
3300–3310		X	X	X	X	X	Cb & Qtz
3400–3410							
3500–3510	X			X	X		Cb
3600–3610	X		X		X	X	Cb & Ep
3700–3710	X			X	X	X	Cb
3800–3810						X	Cb &Anh
3900–3910							
4000–4010				X	X	X	Cb
4100–4110		X	X				
4200–4210	X						
4300–4310		X	X				
4400–4410	X	X	X			X	Cb & Qtz
4500–4510	X	X	X	X	X	X	Cb
4600–4610	X	X	X			X	Cb
4700–4710	?	X	X			X	Cb, Anh, & Qtz
4800–4810	X	X	X	X	X		
4900–4910	?	X	X				
5000–5010	?	X	X		X		
5100–5110	?	X			X		
5200–5210	X	X	X		X	X	Cb
5300–5310	X	X	X	X	X	X	Cb & Anh
5400–5410		X	X	X	X		
5500–5510		X	X		X		
5600–5610		X	X	X	X	X	Cb
5700–5710	?	X		X	X	X	Cb
5800–5810		X	X	X	X		
5900–5910		X	X	X	X	X	Cb
6000–6010	?	X	X	X	X	X	Cb
6100–6110		X	X	X	X	X	Cb
6200–6210	?	X	X		X	X	Cb
6300–6310		X	X	X	X		Cb
6400–6410		X	X		X	X	Cb
6500–6510		X	X	X	X	X	Cb
6600–6610		X	X	X	X	X	Cb, Anh, & Chl
6700–6710		X	X	X	X	X	Cb & Anh
6900–6910		X	X		X		
7000–7010		X	X	X	X	X	Cb
7100–7110		X	X		X	X	Cb
7200–7210		X	X		X		
7300–7310		X	X		X	X	Cb
7400–7410		X	X		X	X	Chl
7500–7510	X	X	X	X	X	X	Cb & Anh

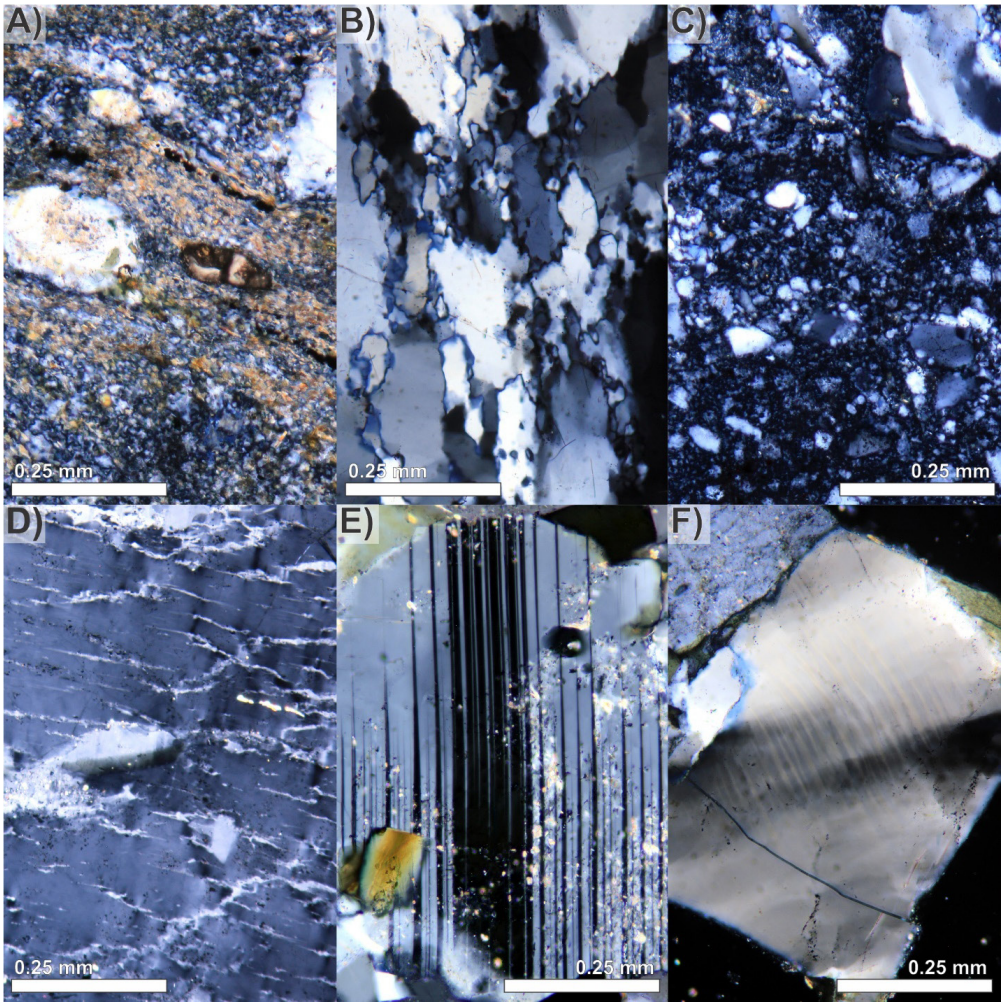

Figure 12. *Cross-polarized light photomicrographs of some of the microstructures observed in the plutonic rocks of well 58-32.* ***(A)*** *Mylonite at 4200–4210 ft.* ***(B)*** *Dynamically recrystallized quartz at 7500–7510 ft.* ***(C)*** *Cataclasite at 7500–7510 ft.* ***(D)*** *Perthite at 7400–7410 ft.* ***(E)*** *Deformation twins in plagioclase at 6300–6310 ft.* ***(F)*** *Quartz grain that displays both undulatory extinction and deformation lamellae at 3300–3310 ft.*

Alluvial deposits. Samples 4380–4400 to 5440–5450 ft

The cuttings from this interval are mostly composed of large (up to at least gravel-size) angular to sub-rounded lithic clasts. Lithic clasts are dominantly composed of plutonic rocks with variable textures, primary minerals and alteration assemblages, with less abundant andesite lava flow and ash-flow tuff clasts, as well as rare vein fragments. The fine-grained matrix is composed of variable proportions of clay (illite, chlorite and smectite) and carbonate (calcite ± dolomite) minerals. Minor carbonate cement is observed at the edges of the clasts or binding clasts together. This unit also contains minor siltstone and fine-grained sandstone with rare fossils, and anhydrite (as nodules and/or laths) with rare chalcedony replacement textures.

Rhyolite ash-flow tuff and tuffaceous sediments. Samples 5640–5650 to 6990–7000 ft

This unit is a mix of rhyolite ash-flow tuff and tuffaceous siltstone and sandstone. The lower part of this unit from 6440–6450 to 6990–7000 ft contains a higher proportion of ash-flow tuff cuttings while the upper part has a higher proportion of tuffaceous sediments.

The rhyolite ash-flow tuffs are moderately to densely welded, with few shard or pumice textures preserved. The cuttings are variable in texture and mineralogy ranging from crystal-rich to crystal-poor, with resorbed quartz, plagioclase and rare sanadine phenocrysts, and chlorite pseudomorphs of ferromagnesian phenocrysts. The groundmass contains variable proportions of quartz, illite, and K-feldspar most commonly as a fine-grained and equigranular groundmass, with less common spherulitic and granophyric devitrification textures.

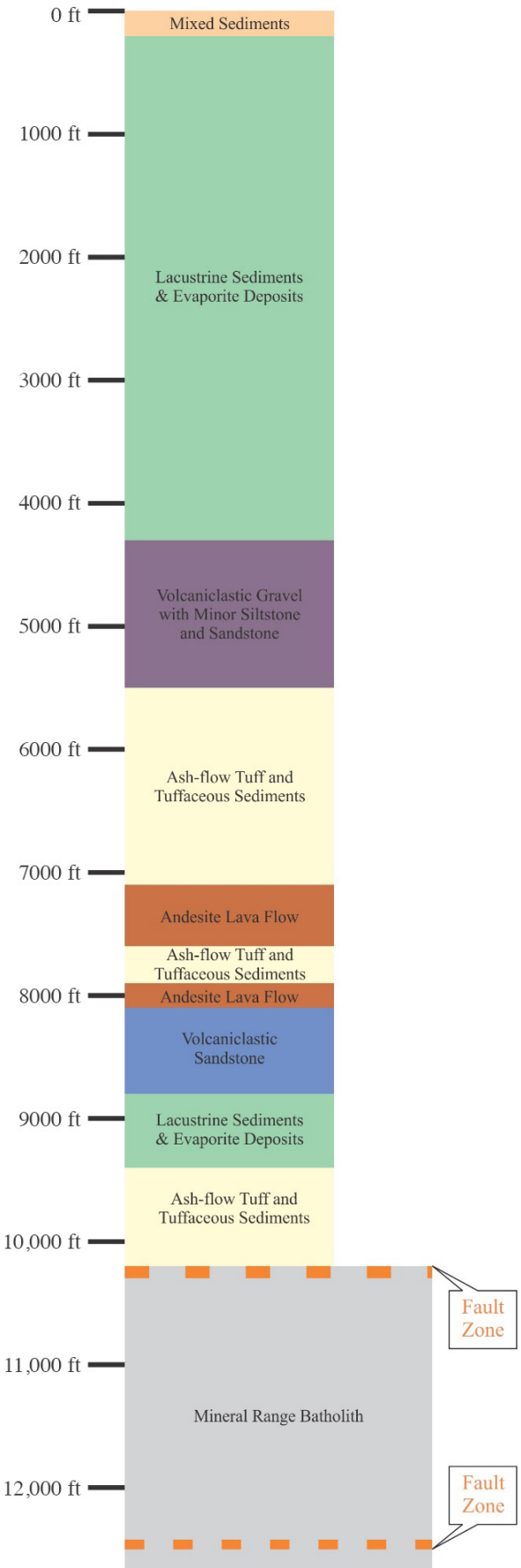

Figure 13. *Stratigraphic column of well Acord-1 constructed from petrographic analyses of cuttings collected at ~50 to 300 ft intervals.*

The sediments consist dominantly of siltstone with detrital quartz, feldspar, and mica grains (mica would have been classified as illite in XRD analyses) and lithic clasts dominantly composed of texturally variable ash-flow tuff with less abundant andesite lava flow and plutonic clasts in fine-grained clay (chlorite and illite ± interlayered illite smectite ± smectite) and/or carbonate (calcite ± dolomite) matrix that is commonly hematite stained. Minor anhydrite is observed as nodules in siltstone.

Silicification of tuff cuttings is commonly observed, but there was no direct evidence of in situ silicification after deposition (i.e., no silicification of fine-grained sedimentary matrix or open-space fillings of quartz or chalcedony that were not contained within a clast).

Andesite lava flow. Samples 7220–7250 to 7540–7550 ft

The samples from this unit consist of porphyritic fine- to medium-grained andesite lava flows with plagioclase, biotite, and clinopyroxene phenocrysts in a fine-grained groundmass composed of plagioclase laths with interstitial K-feldspar and clinopyroxene.

The rock itself is not very altered, there is not much clay in the sample (XRD) and the clinopyroxene grains are often preserved (usually the first mineral in this assemblage to alter/weather), but there is significant secondary silica precipitation in open spaces that resulted from brecciation. Open-space silica is observed as chalcedony, quartz after chalcedony, and anhedral to euhedral quartz. Calcite and rare prehnite are observed filling open space after earlier silica deposition. Calcite veins are also observed cutting earlier sheared/brecciated and silicified chips. Chips containing euhedral quartz growing into open space suggests remnant porosity in this lithology.

Plagioclase is partially altered to albite, K-feldspar, and quartz. Biotite is partially altered to interlayered chlorite/smectite and hematite. Clinopyroxene is partially altered to interlayered chlorite/smectite, quartz, titanite, calcite, and hematite.

Rhyolite ash-flow tuff. Sample 7740–7750 ft

This sample consists of moderately welded, crystal-rich, lithic-poor ash-flow tuff containing plagioclase, sanidine, biotite, and rare quartz phenocrysts, as well as fine-grained quartz pseudomorphs (± hematite) of a ferromagnesian phenocryst. Biotite is often partially altered to hematite. The groundmass contains abundant shards and pumice (fiamme). The shards have been altered to quartz (after chalcedony) and rare analcime. The fine-grained groundmass is K-feldspar- and quartz-rich with a mottled texture. Sparse lithic fragments were derived from andesite lava flows.

The sample contains abundant secondary quartz as replacement of minerals and volcanic glass, as well as open-space fillings. Anhedral quartz is most commonly observed in veins and is likely after chalcedony or opal (i.e., recrystallized). Rare analcime is the last mineral to be deposited in the veins.

Andesite lava flow. Sample 7990–8000 ft

This sample is composed of medium- to coarse-grained andesite flows that have sparse clinopyroxene phenocrysts in a mostly crystalline groundmass consisting of interlocking equigranular plagioclase laths and clinopyroxene, with interstitial K-feldspar and quartz. Plagioclase is partially altered to illite and calcite. Clinopyroxene is partially altered to smectite, hematite, and calcite.

Moderate shearing and minor veining are observed in this sample. Sheared chips are hematite stained. The majority of the open space in the sample appears to be primary including vesicles/amygdules. The sample is cut by several generations of veins: 1) early calcite (botryoidal to euhedral) ± hematite; 2) calcite without hematite; and finally 3) chalcedony followed by quartz. A similar succession of mineralization is recorded in amygdules with quartz precipitating last.

Volcaniclastic sediments. Samples 8240–8250 to 8740–8750 ft

This unit generally consists of volcaniclastic sandstone composed of mineral grains, texturally variable andesite lava flow clasts, and ash-flow tuff clasts in a clay-rich matrix and less commonly calcite cement. Fine-grained quartz with less abundant chalcedony and chlorite fill open pore space. Silicification is also observed. Calcite veins cut the silica deposition and alteration.

Lacustrine sediments and evaporite deposits. Samples 8940–8950 to 9340–9350 ft

This unit is dominantly composed of matrix-supported siltstone consisting of mineral grains and lithic fragments in a clay-rich (interlayered illite/smectite and chlorite ± illite) and/or fine-grained carbonate (dolomite>calcite) matrix. Lithic fragments are derived from ash-flow tuffs (clay altered pumice with remnant vesicular textures and glass shards), andesite lava flows, and plutonic rocks. Preserved shard textures are observed within the fine-grained clay- and/or carbonate-rich matrix. Less commonly anhydrite or calcite cement clasts. This unit contains abundant anhydrite (up to 39 wt% at 9340–9350 ft) as nodules, laths, and thin beds that are partially replaced by chalcedony and quartz. Euhedral rhombohedrons of dolomite are associated with quartz replacements of anhydrite.

Rhyolite ash-flow tuff and tuffaceous sediments. Samples 9540–9550 to 10,140–10,150 ft

The first sample above the granite is composed of equal parts extensively sheared and altered plutonic rock and densely welded ash-flow tuff with minor volcaniclastic sediments. The upper three samples in this unit are composed of ash-flow tuff and tuffaceous sediments.

Trace amounts of tourmaline and epidote are in the sample just above the granite, but they are exclusively within fine-grained plutonic rock chips with no evidence of high-temperature hydrothermal alteration or contact metamorphism observed in the tuff or tuffacous sediments that lie above the thick granite body.

The ash-flow tuff cuttings are densely to non-welded and contain resorbed quartz and plagioclase phenocrysts. The groundmass contains abundant illite-replaced fiamme in the upper part of this unit. In the lower samples, the groundmass is often silicified with a matrix composed of fine-grained quartz with minor illite and K-feldspar.

The volcaniclastic sediments range from silt to gravel-size and consist of mineral grains and lithic fragments in a fine-grained clay-rich matrix with less common fine-grained calcite matrix. The lithic clasts are dominantly composed of ash-flow tuff with less abundant lava flows and plutonic rocks. Pumice fragments are fairly common with preserved vesicular textures that have been extensively altered to interlayered illite/smectite and illite. Plagioclase in ash-flow tuff and lava flow clasts has been partially altered to calcite and anhydrite. Ferromagnesian minerals have been replaced by chlorite. Siltstone cuttings contain anhydrite nodules that may be partially replaced by quartz and/or chalcedony.

Mineral Mountains Batholith. Samples 10,190–10,200 to 12,640–12,650 ft

Cuttings from 10,140–10,150 to 12,640–12,650 ft are composed of plutonic rocks of the Mineral Mountains Batholith. The dominant lithologies encountered in Acord-1 are granite and granodiorite (Figure 14). The vast majority of these lithologies are coarse-grained and composed of equigranular, interlocking plagioclase, K-feldspar, and quartz with minor hornblende and biotite, as well as accessory magnetite/ilmenite, titanite, apatite and zircon (Figure 14A and B).

Minor occurrences of texturally distinct porphyritic intrusive rock with a fine-grained groundmass that range in composition from granite to diorite are observed in samples from 10,190–10,200 ft, 12,090–12,100 ft and 12,240–12,250 ft. Their localized occurrences, minor abundances within the cuttings samples, distinct textures, and relative lack of alteration and deformation compared to the coarser-grained lithologies suggest that these are younger dikes that cut the batholith.

Evidence of brittle deformation such as shearing and brecciation is commonly observed in the cuttings (Figures 15 and 16) and is interpreted to be the result of multiple episodes of tectonic activity. The most intensely deformed of these samples are interpreted as fault zones (Figure 13).

The upper contact between the plutonic rock and the ash-flow tuff/tuffaceous sediments is interpreted as an unconformity with volcanic and volcaniclastic rock deposited on a low-angle fault zone. There is comparatively little deformation in the overlying sedimentary/volcanic units. The lack of contact metamorphism in the lithologies overlying the thick sequence of plutonic rock precludes this as a plutonic contact. The uppermost granitic basement samples are sheared (10,190–10,200 ft) with abundant cataclasite, and a brecciated zone (10,290–10,300 ft) dominated by open-space fillings of quartz and calcite (69 wt% by XRD) with less abundant chlorite, illite, anhydrite, and fluorite (Figure 16A).

Near the bottom of the well at 12,440–12,450 ft another shear zone composed dominantly of cataclasite (Figure 15A) separates medium-grained granitic rock above from finer-grained, compositionally banded plutonic rock with more abundant ferromag-

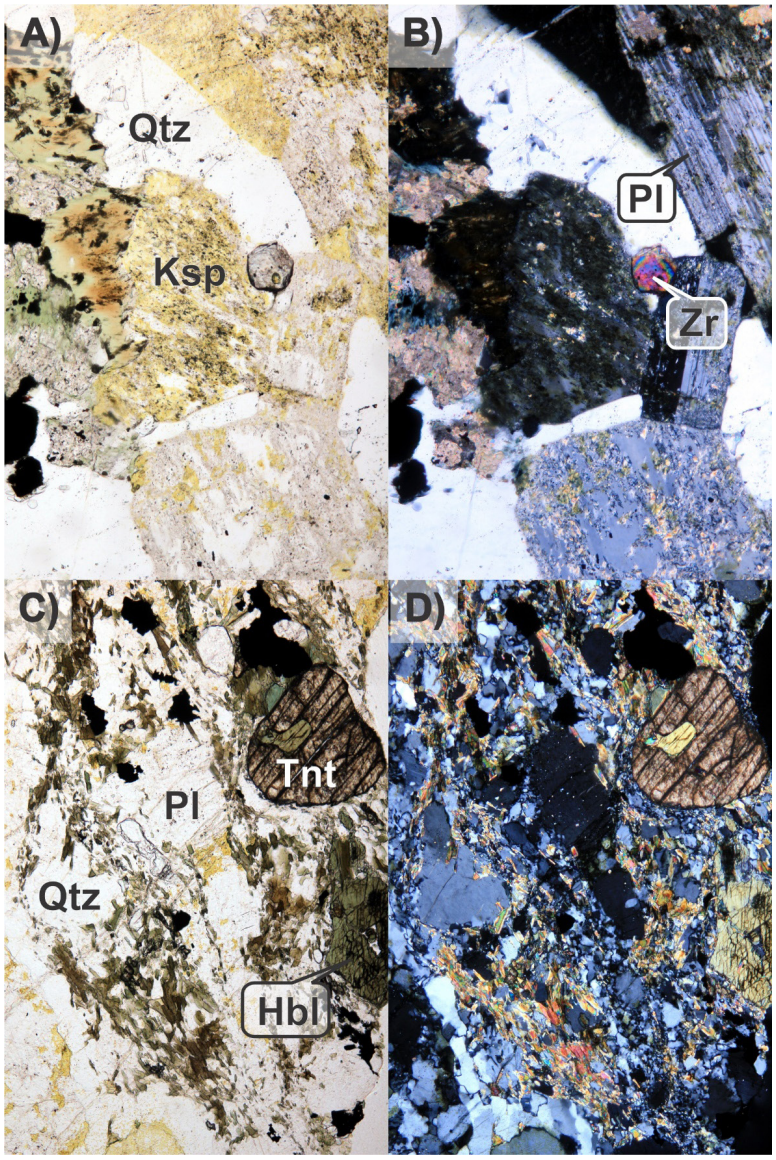

Figure 14. (A&B) *Representative photomicrographs of granite from 12,140–12,50 ft in Acord-1.* ***(C&D)*** *Representative photomicrographs of the finer-grained, compositionally banded granodiorite which contains more ferromagnesian minerals.* ***(A&C)*** *are in plane-polarized light,* ***(B&D)*** *are in crossed-polarized light. Vertical field of view is 1.6 mm in all.*

nesian minerals below (Figure 14B). The deeper, finer-grained plutonic rock displays fewer deformation textures and contains fewer alteration minerals than the medium-grained rocks above. Unlike the upper shear zone, alteration is less prominent and the overall mineralogy more closely resembles unaltered rock.

Secondary minerals in the plutonic rocks of Acord-1 are generally more abundant in cuttings that show evidence of brittle deformation. Plagioclase is variably altered to illite, calcite, K-feldspar, albite and quartz, as well as rare chlorite and epidote. The ferromagnesian minerals are also variably altered with only trace amounts (<1 wt%) remaining in some samples whereas others contain up to 4 wt% hornblende and/or 2 wt% biotite. Biotite is replaced by chlorite, rutile and hematite, and hornblende by chlorite, calcite and hematite. In contrast, K-feldspar, quartz, apatite, zircon, and titanite are relatively unaltered. However, in the most deformed and altered samples quartz is the only major primary phase without replacement textures (Figure 16C and D). In deformed cuttings, quartz often displays undulatory extinction and contains trains of secondary fluid inclusions along healed fractures.

Quartz and calcite are the most commonly observed open-space filling minerals in veins and brecciated rock (Figure 16A and B). Minor phases include chlorite, illite, and anhydrite. Rare open -pace filling of K-feldspar, pyrite, rutile, fluorite, epidote, and fine-grained, fibrous pseudomorphs of actinolite(?) are also observed.

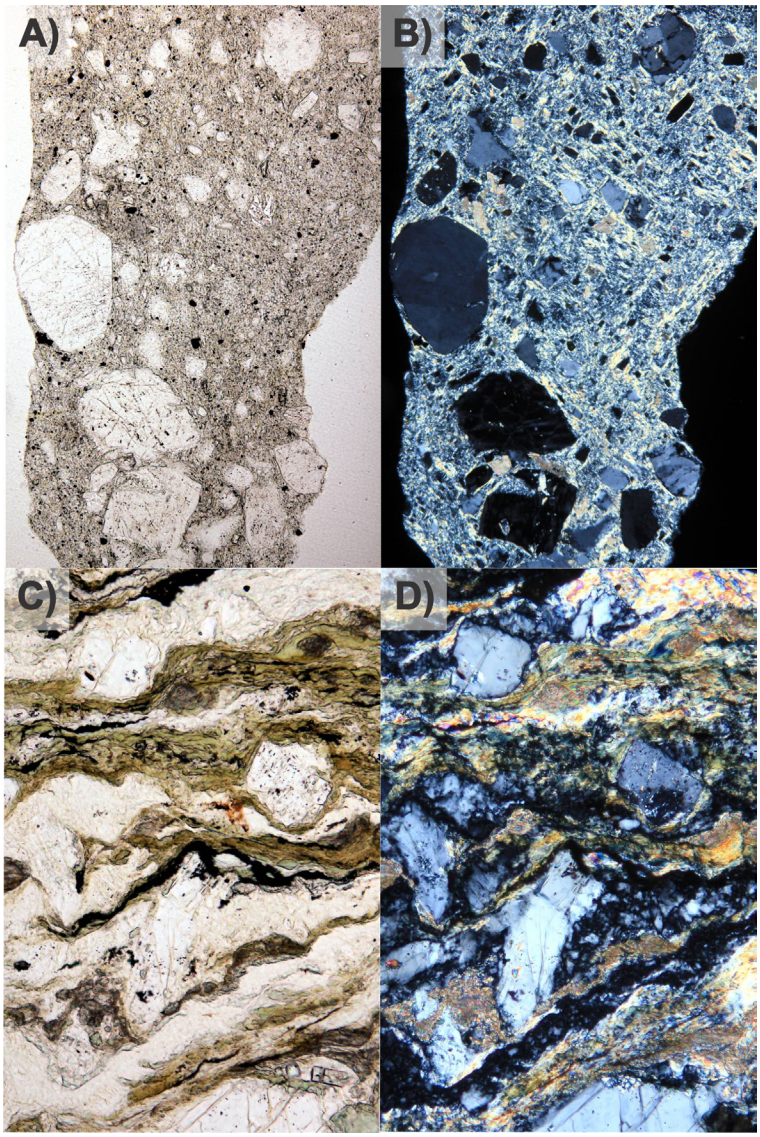

Figure 15. (A&B) *Cataclasite from 12,440–12,450 ft in Acord-1.* ***(C&D)*** *Sheared rock from 10,890–10,900 ft in Acord-1.* ***(A&C)*** *are in plane-polarized light,* ***(B&D)*** *are in crossed-polarized light. Vertical field of view is 1.6 mm in all.*

Several episodes of tectonic deformation and accompanying hydrothermal alteration and open-space mineralization have affected the granitic rocks as evidenced by: 1) rare early epidote (and pseudomorphs of actinolite?) deposited in open space; 2) quartz replacing calcite and anhydrite in veins; 3) calcite and anhydrite veins cutting cataclasite, silica cemented breccia and silicified rock; 4) low abundances of interlayered illite/smectite (from XRD) indicating retrograde argillic overprinting (<225°C); 5) the incorporation of vein fragments in cataclasite; and 6) multiple dikes ranging in composition from granite to diorite that cut extensively deformed rocks.

COMPARISON OF THE PLUTONIC ROCKS IN 58-32 TO THOSE FROM OTHER WELLS AND TO THE ROCKS EXPOSED IN THE MINERAL MOUNTAINS

The Mineral Mountains Batholith, while potentially variable at a fine-scale (foot or meter scale), contains similar lithologies over a wide area, ranging from the deep Acord-1 well in the center of the Milford Valley, to the Mineral Mountains exposed to the east of the FORGE site and in all of the deep geothermal wells in between (Figure 1).

Plutonic rocks encountered in deep geothermal wells (Acord-1, 58-32, 52-21, 9-1 & 14-2) and those that outcrop in the Mineral Mountains have been classified using XRD data (Figure 17). The most common rock types are monzodiorite, quartz monzodio-

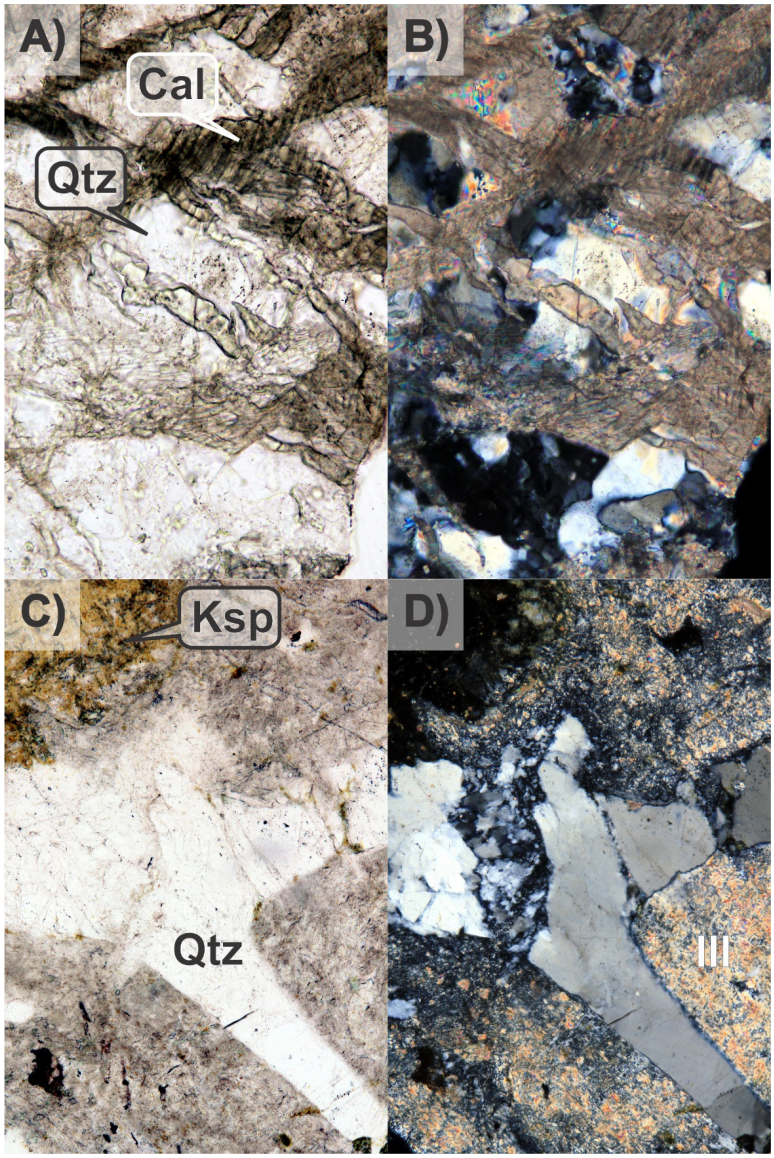

Figure 16. (A&B) *Brecciated quartz vein with open space filled by calcite from 10,290–10,300 ft in Acord-1. Vertical field of view is 0.8 mm.* ***(C&D)*** *Brecciated primary quartz and plagioclase that has been extensively altered to illite from 11,890–11900 ft in Acord-1. Vertical field of view is 1.6 mm.* ***(A&C)*** *are in plane-polarized light,* ***(B&D)*** *are in crossed-polarized light.*

rite, monzonite, quartz monzonite, granite, and granodiorite. The plutonic rocks are dominantly composed of quartz, K-feldspar, and plagioclase that constitutes 57 to 99 wt% of all of the samples analyzed, and average 86 wt%. Primary ferromagnesian minerals including biotite, hornblende, and clinopyroxene are locally abundant and can compose up to 35 wt% of a sample, or as little as <1 wt% (average = 8 wt%). Accessory minerals like titanite and apatite are ubiquitous in the plutonic rocks examined (Min = < 1 wt%, Max = 6 wt%, average = 1 wt%).

Secondary minerals are generally found in low abundance in the plutonic rocks and range from < 1 wt% up to approximately14 wt% with an average of 4 wt%. The highest abundances of secondary minerals were observed in the plutonic rocks of Acord-1. The most common secondary minerals are the clay minerals: smectite; interlayered illite/smectite; interlayered chlorite/smectite; illite; chlorite; and kaolinite. Clay minerals are dominantly observed replacing primary plagioclase, biotite, hornblende, and clinopyroxene. Epidote is sporadically observed replacing plagioclase but is often below the limit of detection by XRD analysis (< 1 wt%). Carbonates (calcite > siderite > dolomite) appear sporadically and are observed filling fractures, often with anhydrite and hematite.

The rocks within the FORGE EGS reservoir most closely resemble samples from outcrop just to the east of the Roosevelt geothermal field, and some of those in well 9-1, Acord-1 and 14-2.

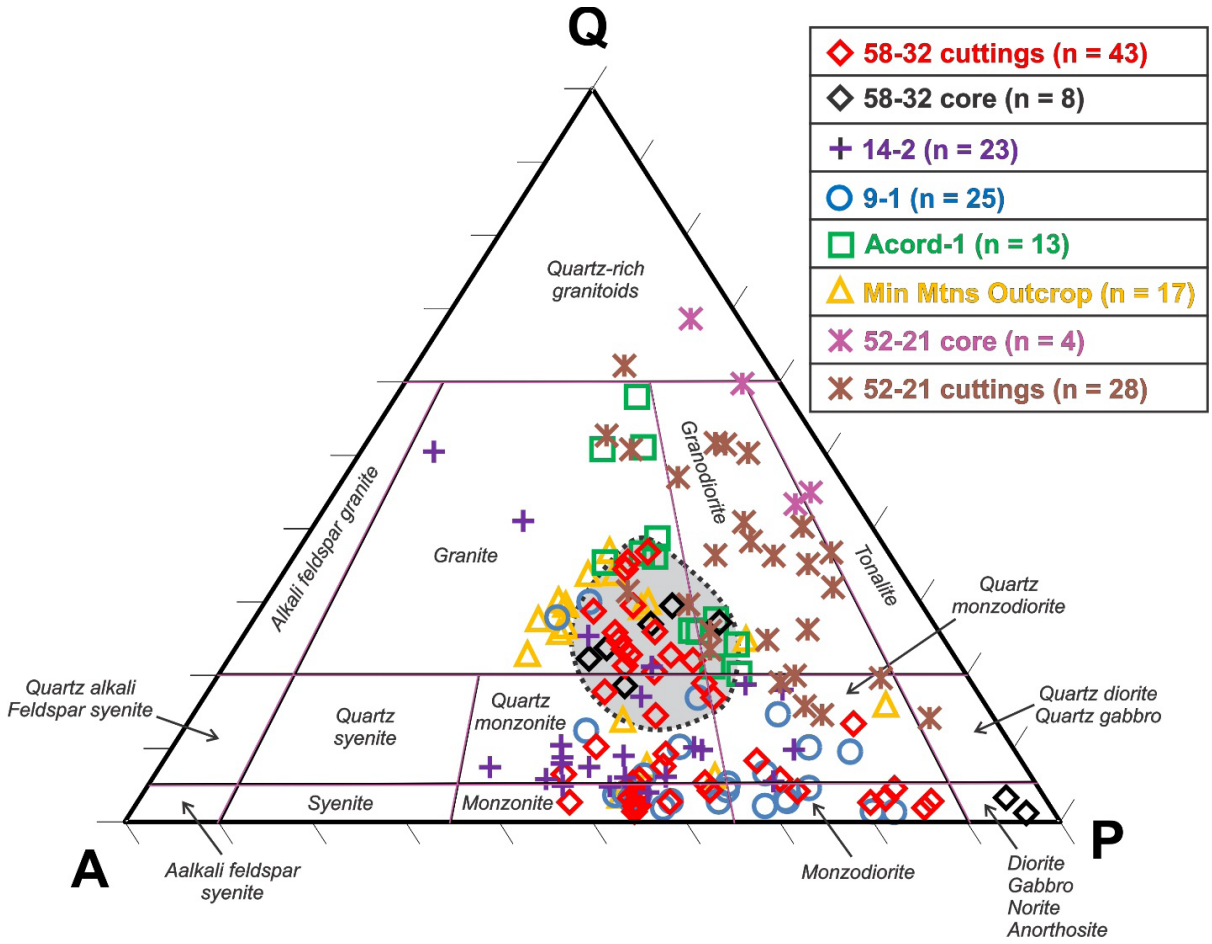

Figure 17. *XRD data from the plutonic rocks of the Mineral Mountains Batholith from deep geothermal wells and outcrop. The data have been normalized to 100 weight percent quartz (Q), K-feldspar (A), and plagioclase (P) and plotted on the IUGS classification diagram (Le Maitre et al., 1989). The majority (15 of 18) of the analyzed samples from within the EGS reservoir are within the gray shaded area and consist of granite, granodiorite, quartz monzonite, and quartz monzodiorite. XRD data from 14-2, 9-1, and Acord-1 come from cuttings.*

CONCLUSIONS

The FORGE site is located on the gently sloping east side of the Milford basin. From the surface to 3176 ft depth, well 58-32 encountered coarse-grained alluvial-fan deposits. To the west, in Acord-1, the basin fill consists of lacustrine sediments, evaporite deposits, volcaniclastic deposits, ash-flow tuff, tuffaceous sediments and andesite lava flows. In well 58-32, FMI logs indicate the basin-fill deposits are undeformed and dip gently to the west mimicking the topography of the plutonic rocks.

The contact between the basin fill and the Mineral Mountains Batholith is interpreted as an unconformity separating plutonic rocks exposed in the footwall of a normal fault from the overlying sediments and volcanic rocks of the basin fill (see Bartley et al., 2019). The absence of high-temperature secondary minerals in the sediments overlying the plutonic rocks precludes this as an intrusive contact. Strong brittle deformation is observed in the rhyolite that separates the alluvium above from the plutonic rock below in well 58-32. In Acord-1 where the unconformity is ~7000 ft deeper, minor brittle deformation is observed in the overlying sediments and volcanic rock when compared to the extensive shearing and brecciating that has impacted the upper portions of the plutonic basement. Coleman and Walker (1994) suggested 30° to 50° of eastward tilting has occurred since 8 to 9 Ma in the western Mineral Mountains which may account for the modern gentle dip of the unconformity beneath the Milford Valley.

The analyzed samples of the Mineral Mountains Batholith from deep geothermal wells and outcrop are composed of plagioclase, quartz, K-feldspar, biotite, hornblende, titanite, apatite, magnetite/ilmenite, and zircon ± clinopyroxene. Variations in bulk composition/mineralogy and texture are observed across the Mineral Mountains Batholith, within each well, and at the outcrop and core scale; however, the rocks within the EGS reservoir are fairly homogeneous and plot primarily within the

granite and quartz monzonite fields of the IUGS classification diagram with minor granodiorite, quartz monzodiorite, and fine-grained banded diorite. With the exception of the diorite in the lower core of well 58-32, the vast majority of the EGS reservoir samples analyzed consist of 90 to 97 wt% coarse-grained, interlocking quartz, K-feldspar, and plagioclase.

Alteration minerals in the plutonic rocks of 58-32 are relatively sparse and decrease in abundance with depth, suggesting an accompanying decrease in permeability. Within the EGS reservoir, secondary minerals make up only a few wt% of the samples on average. Clay minerals are the most common secondary minerals observed in the plutonic rock, with illite and chlorite being most abundant. In geothermal systems, the expected temperature stability ranges of the clay minerals are as follows: at <180°C smectite is stable; at >180°C and <220°C interlayered clays are stable; and at >220°C chlorite and illite are stable (Henley and Ellis, 1983). Traces (<1 wt% by XRD) of smectite and interlayered chlorite/smectite where observed in the deeper part of the well at temperatures >180°C; however, expandable clay minerals are found outside of their expected stability range in low-permeability rocks. Illite and to a lesser extent chlorite are found throughout the batholith and are well below their stability range, suggesting that they are remnants of an earlier alteration episode.

Open-space mineralization was intermittently observed within the EGS reservoir. Observed open-space-filling minerals are calcite, anhydrite, epidote, quartz, chlorite, and plagioclase. Epidote is sporadically observed filling open space and replacing plagioclase. In geothermal systems, epidote typically forms at temperatures greater than 240° to 260°C (Browne, 1978; Reyes, 1990) far above the maximum recorded temperature in well 58-32 of 197°C. The occurrence of epidote, so far outside of its stability range, suggests it too is a remnant of an older episode of alteration.

Carbonates, anhydrite, and the expandable clay minerals would all be expected to form under in situ conditions. Calcite and anhydrite, the most common open-space-filling minerals in the EGS reservoir, both display retrograde solubility and precipitate on heating, suggesting that the fluids within the EGS reservoir are downward percolating.

REFERENCES

Aleinikoff, J.N., Nielson, D.L., Hedge, C.E., and Evans, S.H., 1986, Geochronology of Precambrian and Tertiary rocks in the Mineral Mountains, south-central Utah: U. S. Geological Survey Bulletin 1622, p. 1–12.

Bartley, J.M., 2019, Joint patterns in the Mineral Mountains intrusive complex and their roles in subsequent deformation and magmatism, *in* Allis, R., and Moore, J.N., editors, Geothermal characteristics of the Roosevelt Hot Springs system and adjacent FORGE EGS site, Milford, Utah: Utah Geological Survey Miscellaneous Publication 169-C, 13 p., 1 appendix, https://doi.org/10.34191/MP-169-C.

Browne, P. R. L. (1978). Hydrothermal alteration in active geothermal fields. Annual review of earth and planetary sciences, 6 (1), 229–248.

Coleman, D.S., 1991, Geology of the Mineral Mountains Batholith, Utah: Lawrence, University of Kansas, Ph.D. dissertation, 219 p.

Coleman, D.S., and Walker, J.D., 1992, Evidence for the generation of juvenile granitic crust during continental extension, Mineral Mountains Batholith, Utah: Journal of Geophysical Research, v. 97, no. B7, p. 11,011–11,024.

Coleman, D.S., and Walker, J.D., 1994, Modes of tilting during extensional core complex development: Science, v. 263, no. 5144, p. 215–218.

Fournier, R.O., 1985, The behavior of silica in hydrothermal solutions; *in* Berger, B.R., and Bethke, P.M., editors, Geology and geochemistry of epithermal systems: Reviews in Economic Geology, v. 2, p. 45–62.

Henley, R.W., and Ellis, A.J., 1983, Geothermal systems ancient and modern—a geochemical review: Earth-science reviews, v. 19 no. 1, p. 1–50.

Kirby, S.M., Knudsen, T.R., Kleber, E., and Hiscock, A., 2018, Geologic map of the Utah FORGE area: Utah Geological Survey Contract Deliverable for DOE project number DE-EE0007080, scale 1:24,000, 2 plates, 13 p.

Le Maitre, R.W., Dudek, P., Keller, A., Lameyre, J., Le Bas, J., Sabine, M.J., Schmid, P.A., Sorensen, R., Streckeisen, H., Woolley, A., and Zanettin, A.R., 1989, A classification of igneous rocks and glossary of terms—Recommendations of the International Union of Geological Sciences, Sub commission on the Systematics of Igneous Rocks: International Union of Geological Sciences. Blackwell Science, Oxford, p. 236.

Lipman, P.W., Rowley, P.D., Mehnert, H.H.S., Evans, S.H.J., Nash, W.P., and Brown, F.H., 1978, Pleistocene rhyolite of the Mineral Range, Utah—Geothermal and archaeological significance: U.S. Geological Survey Journal of Research, v. 6 no. 1, p. 133–147.

Moore, J.N., Allis, R.G., Nemčok, M., Powell, T.S., Bruton, C.J., Wannamaker, P.E., and Norman, D.I., 2008, The evolution of volcano-hosted geothermal systems based on deep wells from Karaha–Telaga Bodas, Indonesia: American Journal of Science, v. 308 no. 1, p. 1–48.

Moore, D.M., and Reynolds, R.C., 1997, X-ray Diffraction and the Identification and Analysis of Clay Minerals (p. 155). Oxford: Oxford university press.

Reyes, A.G., 1990, Petrology of Philippine geothermal systems and the application of alteration mineralogy to their assessment: Journal of Volcanology and Geothermal Research, v. 43, p. 279–309.

Sander, B., 1930, Gefugekunde der Geteine: Vienna, Springer, 352 p.

Simpson, C., and Wintsch, R.P., 1989, Evidence for deformation-induced K-feldspar replacement by myrmekite: Journal of Metamorphic Geology, v. 7, no. 2, p. 261–275.

Vernon, R.H., 2004, A practical guide to rock microstructure: Cambridge University Press, 594 p.

Walker, F.D.L., Lee, M.R., and Parsons, I., 1995, Micropores and micropermeable texture in alkali feldspars—geochemical and geophysical implications: Mineralogical Magazine, v. 59, no. 3, p. 505–534.

Appendix A: XRD Data Sets

Summary of XRD data from wells 58-32, Accord-1, 52-21, 9-1 and 14-2, as well as outcrop samples from the Mineral Mountains (Table A1). For each XRD data set presented in Table A1 the full XRD data are presented in Tables A2 through A9.

Table A1. *XRD data sets.*

XRD data set	Sample type	XRD analyses
58-32	cuttings	78
58-32	core	8
14-2	cuttings	23
9-1	cuttings	25
Accord 1-26	cuttings	62
52-21	core	4
52-21	cuttings	30
Mineral Mountains	outcrop/ hand sample	17
Total		***247***

***Table A2**. XRD data acquired from cuttings of FORGE well 58-32. Sample depths are shown in the first column (drillers depth). XRD data are given in weight percent of sample, with values rounded to the nearest whole number. Fields marked with tr (trace) indicate that this mineral is present, but represents less than 1 wt% of the sample or that it was observed in the clay-sized fraction but not the bulk pattern, and/or it was observed in thin section. Where possible, the composition of interlayered chlorite/smectite was determined based on a comparison of air-dried and glycolated clay-size fraction diffractograms and is indicated in the column "% chlorite in C/S."*

58-32 Cuttings Depth (ft)	**Plagioclase**	**K-feldspar**	**Quartz**	**Biotite**	**Titanite**	**Hornblende**	**Apatite**	**Clinopyroxene**	**Smectite**	**Interlayered Chlorite-Smectite**	**% chlorite in C/S**	**Chlorite**	**Illite**	**Kaolinite**	**Epidote**	**Calcite**	**Dolomite**	**Siderite**	**Hematite**	**Anhydrite**
100–110	40	44	17						tr				tr							
200–210	42	33	20	tr					tr				4						tr	
300–310	39	34	26						tr				tr			2				
400–410	35	39	20	1					1				4						tr	
500–510	35	39	21	tr					tr				4						tr	
600–610	35	49	16						tr				tr						tr	
700–710	36	43	20						tr				tr						tr	
800–810	38	43	18						tr				tr						tr	
900–910	31	41	28						tr				tr						tr	
1000–1010	37	34	24	2					tr				3						tr	
1100–1110	40	36	24						tr				tr						tr	
1200–1210	36	39	25						tr				tr						tr	
1300–1310	37	37	25						tr				tr						tr	
1400–1410	38	35	26						tr				tr						tr	
1500–1510	34	38	27						tr				tr						tr	
1600–1610	35	38	26						tr				tr						1	
1700–1710	33	38	28						tr				tr						tr	
1800–1810	36	35	25	tr					tr				3						1	
1900–1910	34	41	20	tr					tr				3						tr	
2000–2010	34	40	21	tr					tr				4						tr	
2100–2110	37	33	22	3					tr				3						1	
2200–2210	35	34	25	1					tr				4						tr	
2300–2310	35	36	24	1					tr				3						tr	
2400–2410	42	37	15	4					tr				2						1	
2500–2510	35	34	26	2					tr				3						1	
2600–2610	38	37	19	1					tr				3						1	
2700–2710	38	40	18						tr				3						tr	
2800–2810	36	38	20	tr					tr				4						1	
2900–2910	38	37	19	1					tr				4						1	
3000–3010	37	37	20	2					tr				3						2	
3100–3110	38	39	18	1					tr				3						tr	
3170–3180	19	41	34	1					tr				2	1		1				
3180–3190	15	42	38	tr					tr				3	1		tr				
3190–3200	28	47	11	3			tr		tr				5	tr		tr		3	2	tr
3200–3210	40	39	9	3	tr		3		tr				5	tr		tr				
3300–3310	39	44	6	2	tr		3		tr				6	tr		tr				
3330–3340	43	32	2	8	tr		tr		tr				4	2		tr		6	2	tr

***Table A2**. Continued.*

3400–3410	43	48	3	tr	tr		2		tr				3	tr		tr				
3500–3510	49	18	3	16	tr	3	3	5	tr	tr	50	tr	1			tr				
3600–3610	55	12	2	11	2	7	2	5	tr	tr	N/A	1.2	3		tr	tr				
3700–3710	45	18	4	12	tr	1	1	4	tr			1.2	5			tr	2	3	1	1
3800–3810	54	13	2	11	1	6	2	8	tr			tr	2			tr				
3900–3910	51	8	2	11	2	11	2	9	tr	tr	N/A	1.5	2		tr	1				
4000–4010	53	9	1	11	2	8	3	10	tr	tr	N/A	1	2			tr				
4100–4110	46	27	4	6	tr	4	1	5	tr			1	4			2				
4200–4210	54	11	3	15	1	6	1	5	tr			1	2		tr	1				
4300–4310	50	41	2	2	tr	tr	tr		tr	tr	N/A	tr	3			tr				
4400–4410	44	36	3	4	tr	4	tr	4	tr	tr	N/A	1.6	2			tr				
4500–4510	48	40	2	2	tr	2	tr	2	tr	tr	50	tr	2			1				
4600–4610	47	38	5	2	tr	2	tr	2		tr	N/A	tr	4			tr				
4700–4710	49	35	7	2	tr	2	tr	2	tr	tr	50		3			tr				
4800–4810	51	30	4	5	tr	2	tr	3	tr	tr	50	tr	4			tr				
4900–4910	51	42	2	tr	tr	1							3							
5000–5010	51	42	1	1	tr	tr	tr						3			tr				
5100–5110	54	39	3	tr	tr	1	tr						2			tr				
5200–5210	39	34	24	1	tr	tr	tr					tr	2			tr				
5300–5310	50	41	5	2	tr	tr	tr			tr			2		tr	tr				
5400–5410	34	33	27	1	tr	1	tr						3			tr				
5500–5510	35	28	35	tr	tr	tr	tr					tr	1			tr				
5600–5610	39	32	19	4	tr	1	1		tr			tr	3		tr	tr				
5700–5710	36	25	35	tr	tr	tr	tr		tr				2		tr	tr				
5800–5810	35	29	34	tr	tr	tr	tr						1	tr		tr				
5900–5910	39	30	29	tr	tr	tr	tr	tr					1			tr				
6000–6010	59	27	8	2	tr	tr	tr						3			tr				
6100–6110	50	42	3	1	tr	tr	tr						3			tr				
6200–6210	53	37	9	tr	tr	tr	tr						tr			tr				
6300–6310	38	33	25	1	tr	tr	tr						3	tr		tr				
6400–6410	41	28	24	2	tr	tr							4			tr				
6500–6510	40	33	22	1	tr	tr	tr						2			tr				
6600–6610	41	38	17	1	tr	tr	tr					tr	2							
6700–6710	69	15	13	tr	tr	tr	tr			tr	50	1	tr	tr						
6900–6910	44	29	21	1	tr	tr	tr					tr	3		tr					
7000–7010	48	26	17	1	tr	1	tr			tr	N/A	tr	4		tr	tr				
7100–7110	47	34	14	2	tr	tr	tr						3		tr					
7200–7210	44	31	19	2	tr	tr			tr	tr	50	tr	2		tr	tr				
7300–7310	40	32	21	3	tr	tr	tr			tr	50	tr	3		tr	tr				
7400–7410	50	26	16	3	tr	2	tr			tr	N/A	tr	2		tr	tr				
7500–7510	47	28	21	2	tr	tr	tr		tr	tr	50	tr	1			tr				

***Table A3**. XRD data acquired from core of FORGE well 58-32. Sample depths are shown in the first column (drillers depth). XRD data are given in weight percent of sample, with values rounded to the nearest whole number. Fields marked with tr (trace) indicate that this mineral is present, but represents less than 1 wt% of the sample, or that it was observed in the clay-size fraction but not the bulk pattern, and/or it was observed in thin section. Where possible, the composition of interlayered chlorite/smectite was determined based on a comparison of air-dried and glycolated clay-size fraction diffractograms and is indicated in the column "% chlorite in C/S."*

58-32 Core Depth (ft)	**Plagioclase**	**K-feldspar**	**Quartz**	**Biotite**	**Titanite**	**Hornblende**	**Apatite**	**Smectite**	**Interlayered Chlorite-Smectite**	**% chlorite in C/S**	**Chlorite**	**Illite**	**Calcite**
6801.15 H	47	21	26	5	tr	tr	tr		tr	50		tr	
6802.18 V-A	40	25	27	3	tr	tr	tr		tr	N/A		3	
6809.00 H	37	34	22	3	tr	tr			tr	50		2	
6810.15 V-A	37	37	21	4	tr				tr	50		tr	
7442.60 H	62	3	2	15	2	16	1	tr				tr	tr
7445.40 V-C	56	2	1	12	1	24	2				3	1	tr
7447.95 V-B	38	27	24	4	tr	tr	tr		tr	50	1	4	
7451.85 H	42	36	18	3	tr	tr			tr	N/A	tr	tr	

***Table A4**. XRD data acquired from cuttings of well 14-2. Sample depths are shown in the first column (drillers depth). XRD data are given in weight percent of sample, with values rounded to the nearest whole number. Fields marked with tr (trace) indicate that this mineral is present, but represents less than 1 wt% of the sample, or that it was observed in the clay-size fraction but not the bulk pattern, and/or it was observed in thin section. Where possible, the composition of interlayered illite/smectite was determined based on a comparison of air-dried and glycolated clay-size fraction diffractograms and is indicated in the column "% illite in I/S."*

14-2 Cuttings Depth (ft)	**Plagioclase**	**K-feldspar**	**Quartz**	**Biotite**	**Titanite**	**Hornblende**	**Apatite**	**Smectite**	**Interlayered Illite-Smectite**	**% Illite in I/S**	**Chlorite**	**Illite**	**Kaolinite**	**Calcite**	**Hematite**
590–600	42	48	5	3	tr		tr	tr				2		tr	
740–750	40	46	8	3	tr		tr	tr				2		tr	
1010–1020	32	33	22	8	tr	tr	tr	tr			1	3		tr	
1240–1250	34	54	7	2	tr			tr				2			
1520–1530	42	43	7	4	tr		tr	tr				2		1	
1720–1730	7	36	44	2				tr	tr	70–80		4	5	tr	tr
1995–2000	21	34	38	1	tr				tr	70–80		5			tr
2240–2245	40	29	19	5	tr		tr		tr	80	2	4			
2495–2500	51	30	9	4	tr		tr		tr	80–90	2	4		tr	
2755–2760	48	16	14	12	1	1	1				tr	5		2	
2955–3000	57	20	9	8	tr		tr				tr	2		1	
3245–3250	49	35	6	3	tr		tr				1	6		1	
3495–3500	37	43	9	1	tr		tr				2	5		tr	
3745–3750	49	38	4	tr	tr		tr				3	3		tr	
3995–4000	50	30	9	4	tr		tr				1	2		2	
4245–4250	39	45	7	2			tr				2	5		tr	
4495–4500	39	48	5	tr	tr		tr				2	4		1	
4745–4750	46	42	5	2	1						1	2		2	
4995–5000	38	29	14	5	1		tr				2	8		3	
5245–5250	54	23	5	10	tr	tr	1				tr	4		2	
5495–5500	46	40	6	2	tr	tr					tr	3		1	
5740–5745	45	39	8	4	tr	1	tr				tr	2		tr	
5995–6000	42	18	14	8	tr	10	tr				tr	4		2	

***Table A5**. XRD data acquired from cuttings of well 9-1. Sample depths are shown in the first column (drillers depth). XRD data are given in weight percent of sample, with values rounded to the nearest whole number. Fields marked with tr (trace) indicate that this mineral is present, but represents less than 1 wt% of the sample or that it was observed in the clay-size fraction but not the bulk pattern, and/or it was observed in thin section. Where possible, the composition of interlayered illite/smectite was determined based on a comparison of air-dried and glycolated clay-size fraction diffractograms and is indicated in the column "% illite in I/S."*

9-1 Cuttings Depth (ft)	**Plagioclase**	**K-feldspar**	**Quartz**	**Biotite**	**Titanite**	**Hornblende**	**Apatite**	**Clinopyroxene**	**Smectite**	**Interlayered Illite-Smectite**	**% Illite in I/S**	**Chlorite**	**Illite**	**Calcite**	**Hematite**
760	50	27	4	11	3	tr	1		tr			1	3		
1010	32	33	28	4	tr				tr			tr	2		
1240	26	32	23	6	tr				2			tr	6	3	1
1480	43	34	5	10	1		tr		tr			tr	3	3	tr
1750	46	11	6	12	1	7	1	9	tr			tr	6	2	
2020	39	41	12	4	tr				tr			tr	2	tr	1
2250	42	15	10	10	tr	2	3	10	tr			tr	5	1	2
2500	45	29	9	8	tr	1	tr		tr			tr	3	2	1
2750	42	24	14	7	tr		tr		tr	tr	>90	4	6	2	
3000	48	21	5	13	tr	tr	3		tr			tr	8	2	
3250	46	25	4	13	tr	1	2		tr			tr	7	2	
3450	52	17	8	9	2	6	tr		tr			tr	3	2	
3700	47	41	4	4	tr		tr					tr	2	1	
4010	46	42	4	4	tr		tr		tr			tr	3	2	
4200	51	29	2	12	tr	1	1					tr	3	1	
4500	58	23	3	11	tr	tr	tr					tr	2	1	
4700	55	22	2	14	1	tr	tr					tr	2	2	
5000	47	35	2	7	tr	tr	tr					tr	4	2	
5240	46	32	2	10	1	tr	2		tr			tr	5	2	
5500	45	38	3	9	tr	1	tr		tr			tr	1	1	
5780	46	37	3	7	tr	tr	tr					tr	3	2	
6000	53	24	2	13	tr	3	1					1	1	1	
6200	55	11	1	21	tr	6	2						3	1	
6500	50	12	1	25	tr	4	3						3	tr	
6790	40	14	3	29	1	2	4						5	2	

***Table A6**. XRD data acquired from cuttings of well Acord-1. Sample depths are shown in the first column (drillers depth). XRD data are given in weight percent of sample, with values rounded to the nearest whole number. Fields marked with tr (trace) indicate that this mineral is present, but represents less than 1 wt% of the sample, or that it was observed in the clay-size fraction but not the bulk pattern, and/or it was observed in thin section. Where possible, the composition of interlayered illite/smectite was determined based on a comparison of air-dried and glycolated clay-size fraction diffractograms and is indicated in the column "% illite in I/S."*

Acord-1 Cuttings Depth (ft)	Plagioclase	K-feldspar	Quartz	Biotite	Titanite	Hornblende	Apatite	Clinopyroxene	Magnetite	Smectite	Interlayered Illite-Smectite	% Illite in I/S	Interlayered Chlorite-Smectite	% chlorite in C/S	Chlorite	Illite	Kaolinite	Epidote	Calcite	Dolomite	Hematite	Anhydrite	Prehnite	Rutile	Pyrite	Aragonite	Bassanite	Halite	Analcime
70–100	17	11	28							tr						7	11		27										
320–350	7	7	32							2						7	16		19	10		tr							
590–620	7	11	15							tr						12	tr		21	21						12		1	
830–860	6	9	10							tr						11			14	36		4				7	3		
1070–1100	9	10	15							tr						9			20	25						12			
1340–1350	6	13	13							tr						15			12	20		2				15	5		
1580–1610	6	13	13							tr						15			14	26		5				8			1
1820–1850	4	12	9							tr					tr	13			10	19		13				5	10		4
2090–2120	16	18	27							tr					2	14			10	9						2			2
2330–2360	22	17	35							tr					4	4			13	3									2
2600–2630	17	20	25							tr					3	16			10	4		2				1			2
2840–2850	11	21	35							tr					9	10			14										
3080–3110	10	19	29							tr					3	21			12			6							
3320–3350	7	17	16							2					7	6			11	tr		35							
3590–3600	26	21	31							2					4	6			4	3	tr	2							
3840–3850	11	21	17							3					7	11			14	10	tr	6							
3990–4000	14	21	23							tr					3	17			14	5		4							
4240–4250	14	21	15							4					9	10			12	6	tr	8							
4380–4400	32	25	31							2					2	6			2			tr							
4640–4650	27	31	28							1					5	3			3		2	tr							
4840–4850	31	28	27							1					5	4			2		2	tr							
5040–5050	28	30	30							1					4	3			2		2	tr							
5240–5250	27	34	26							2					4	3			3	tr	1	tr							
5440–5450	20	28	24							3					7	8			8		2	tr							
5640–5650	21	26	25							6					6	6			9		1	tr							
5840–5850	21	30	32							tr	tr	90			6	6			4		2	tr							

Table A6. *Continued.*

6040–6050	16	39	28							tr	tr	90			6	4			2		2	2							
6240–6250	18	29	26							tr	tr	90			7	7			7	2	1	3							
6440–6450	22	26	37							tr	tr	90			6	6			2		1								
6640–6650	25	25	33							tr	tr	90			6	6			3		1	tr							
6840–6850	24	26	34							tr	tr	90			6	5			3		2	tr							
6990–7000	26	31	29							tr	tr	90			3	3			5		1	1							
7220–7250	46	31	10	tr	tr			2		1			1	50		1			4		3		tr						
7540–7550	50	27	15	tr				tr		tr			1	50		1			tr		4								tr
7740–7750	30	35	28	2							tr	50,90			tr	tr			tr		tr								3
7990–8000	41	9	12	tr				9		10						5			8		6								
8240–8250	36	10	23					tr		2	2	90			6	13			5		2								
8340–8350	25	8	27							7	19	90			9	tr			5	tr									
8540–8550	22	11	41								16	50,90			6	tr			4										
8740–8750	24	9	33								24	50,90			5	tr			2	2		tr							
8940–8950	25	9	25								22	50,90			6	tr			3	6		4							
9140–9150	10	9	19								26	50,90			7				5	13		12							
9340–9350	9	5	17								12	90			8				2	8		39							
9540–9550	20	7	26								27	50,90			8				4			7			tr				
9740–9750	23	8	23								4	50,90			9	24			4			5			tr				
9940–9950	18	18	24								3	50,90			13	16			2		1	4			1				
10,140–10,150	33	11	28				tr				tr	90			12	12		tr	1			1			1				
10,190–10,200	11	22	32	tr			tr	tr	tr		tr	50,90			12	12			9		tr	2							
10,290–10,300	6	9	34	tr			tr	tr	tr		tr	50,90			6	8			35		tr	tr							
10,490–10,500	26	18	25	tr	1		tr		tr		tr	90			13	10			5			1							
10,690–10,700	40	21	16	tr	tr	3	tr		1		tr	90			6	8		tr	3			tr							
10,890–10,900	19	12	32	tr	1	tr	tr		1		tr	50,90			11	13		1	7		tr	tr							
11,090–11,100	36	17	20	2	1	1	tr	tr	1		tr	50,90			14	4		tr	3		tr								
11,290–11,300	43	18	19	2	1	2	tr		1		tr	50			2	8		tr	3		tr	tr							
11,490–11,500	16	10	35	tr	tr	4	tr	1	tr		tr	90			8	11		tr	10	1	tr	1							
11,690–11,700	34	18	18	tr	tr	4	tr		tr		tr	90			11	9			5		tr				tr				
11,890–11,900	36	20	20	1	1		tr		1		tr	90			8	6			5		tr								
12,090–12,100	30	19	30	tr	tr		tr		tr		tr	90			6	7			4		tr	1		tr	tr				
12,140–12,150	17	15	33		2	tr	tr				tr	90			6	18			5	1		3		tr					
12,240–12,250	31	20	28	1	tr		tr		1						9	2			3	1		3							
12,440–12,450	25	23	26	tr	1		tr								5	11			1	4		3							
12,640–12,650	43	19	15	4	3	6	tr								4	6			tr			tr							

***Table A7**. XRD data acquired from 52-21 core samples. Sample depths are shown in the first column (drillers depth). XRD data are given in weight percent of sample, with values rounded to the nearest whole number. Fields marked with tr (trace) indicate that this mineral is present, but represents less than 1 wt% of the sample, or that it was observed in the clay-size fraction but not the bulk pattern, and/or it was observed in thin section.*

52-21 Core Depth (ft)/ Sample ID	**Plagioclase**	**K-feldspar**	**Quartz**	**Biotite**	**Titanite**	**Hornblende**	**Apatite**	**Chlorite**	**Illite**	**Calcite**
3578-3583	46	6	40	6	tr	tr	tr	tr	tr	tr
GNS-5	25	5	66	3	tr	tr	tr	tr	tr	tr
GNS-6	35	4	58	3		tr	tr	tr	tr	tr
GNS-7	49	4	43	3	tr	tr	tr	tr	tr	tr

***Table A8**. XRD data acquired from cuttings of well 52-21. Sample depths are shown in the first column (drillers depth). XRD data are given in weight percent of sample, with values rounded to the nearest whole number. Fields marked with tr (trace) indicate that this mineral is present, but represents less than 1 wt% of the sample, or that it was observed in the clay-size fraction but not the bulk pattern, and/or it was observed in thin section. Where possible, the composition of interlayered illite/smectite was determined based on a comparison of air-dried and glycolated clay-size fraction diffractograms and is indicated in the column "% illite in I/S."*

52-21 Cuttings Depth (ft)	**Plagioclase**	**K-feldspar**	**Quartz**	**Biotite**	**Titanite**	**Hornblende**	**Apatite**	**Clinopyroxene**	**Smectite**	**Interlayered Illite-Smectite**	**% Illite in I/S**	**Chlorite**	**Illite**	**Calcite**
230–240	41	32	14	1		3			tr			tr	8	
500–510	34	18	38	5	2	tr	tr		tr				3	
700–710	44	15	14	13	3	9	1		tr			tr	2	
1000–1010	49	13	11	11	2	5	1		tr			2	7	
1230–1240	46	14	11	12	3	9	1		tr			tr	3	
1490–1500	20	18	43	16	tr				tr			tr	3	
1790–1800	23	17	41	14	2				tr			3	tr	
2000–2010	33	10	46	7	tr	tr			tr			1	3	
2240–2250	17	12	47	19	2	1			tr			tr	2	
2490–2500	34	9	45	8					tr			tr	4	
2690–2700	32	16	43	3	tr				tr			1	4	
2990–3000	44	13	35	4	tr							tr	2	
3250–3260	51	9	32	5	tr				tr			tr	2	
3500–3510	48	7	37	4	tr		tr		tr			tr	2	
3730–3740	52	6	33	5	tr	1	tr		tr			tr	1	
3990–4000	49	12	34	3	tr							tr	1	
4240–4250	52	7	28	9	tr	2						tr	tr	
4520–4530	51	12	22	8	1	4	tr					tr	2	
4790–4800	48	4	9	9	1	25	1					tr	2	
4990–5000	46	23	21	4	tr	1			tr			1	3	
5290–5300	44	13	39	2		2			tr			tr	tr	
5490–5500	44	6	34	10	tr	4	tr		tr			tr	2	
5710–5720	53	7	15	4	tr	18	tr		tr			tr	tr	
5910–5920	36	29	29	4	tr	2			tr			tr	tr	
6210–6220	47	16	21	9	tr	2	tr					2	tr	2
6540–6550	40	22	26	7	tr	2	tr					tr	tr	
6740–6750	43	21	23	7	tr	1						tr	4	
6980–6990	39	16	31	6	tr	1			tr	tr	~90%	1	5	1
7260–7270	50	15	16	5	2	8	tr					tr	4	
7490–7500	35	7	42	14	tr							1	tr	

***Table A9**. XRD data acquired from hand samples collected from outcrops in the Mineral Mountains by Mark Gwynn. Rock-type designation is based on mapping by Sibbett and Neilson (2017). XRD data are given in weight percent of sample, with values rounded to the nearest whole number. Fields marked with tr (trace) indicate that this mineral is present, but represents less than 1 wt% of the sample, or that it was observed in the clay-size fraction but not the bulk pattern, and/or it was observed in thin section. Where possible, the composition of interlayered illite/smectite was determined based on a comparison of air-dried and glycolated clay-size fraction diffractograms and is indicated in the column "% illite in I/S."*

Min Mtns Outcrop Sample ID	**Plagioclase**	**K-feldspar**	**Quartz**	**Biotite**	**Titanite**	**Hornblende**	**Apatite**	**Smectite**	**Chlorite**	**Illite**	**Calcite**
1 Tgr	32	38	25	1	tr				tr	2	tr
4 Ts	49	44	3	1	tr					2	tr
6A Tqm	32	28	35	1	tr					3	
7A Tgr	31	36	28	3	tr		tr			1	
7B Tgr	30	43	22	3	tr					2	
8 Xbg	35	25	26	10	1	tr	tr		1	1	tr
10 gd	32	38	24	1	tr					4	tr
11 gd	29	41	27	1						2	tr
12 hgn	34	25	24	2	tr	11	tr		tr	3	tr
13 Tgr	32	33	33	tr				tr		1	
14 Tg	53	30	5	5	1	1	tr			4	
15 Tbg	29	36	28	tr	tr		tr		2	4	
16 hgn	56	8	12	4	1	17	tr			tr	
17 Xbg	38	32	11	5	tr	11	tr			1	
18	37	29	5	2	tr		2	tr	11	10	3
19	33	29	32	2	tr			tr	1	3	
20	46	18	21	5	tr	6	tr	tr	1	1	

Appendix B: Representative photomicrographs of basin-filling lithologies encountered in Acord-1

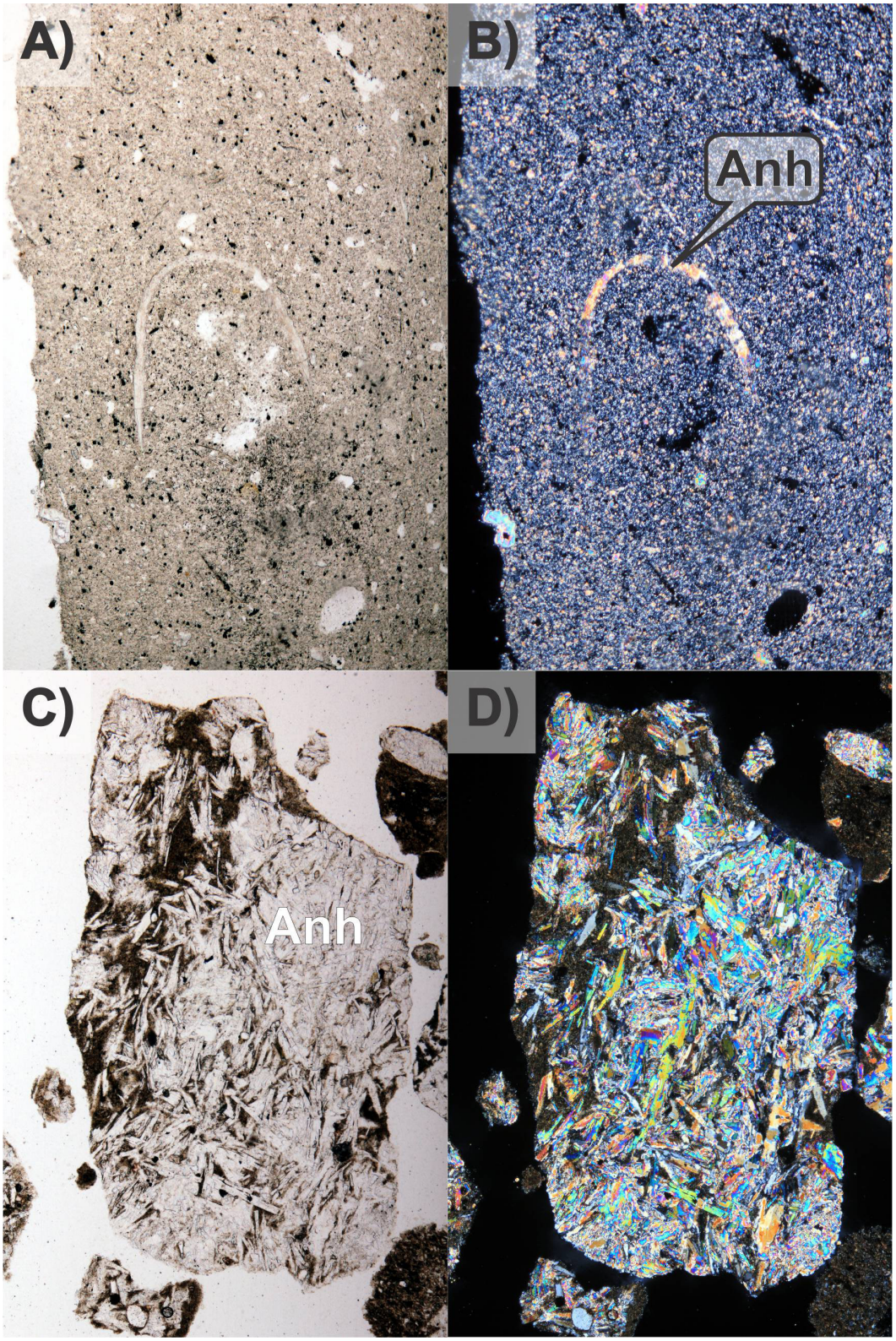

Figure B1. 320–350 to 4240–4250 ft: *Representative photomicrographs of lacustrine sediments and evaporite deposits.* ***(A&B)*** *Anhydrite replaced fossil in siltstone (1070–1100 ft). Vertical field of view is 1.6 mm.* ***(C&D)*** *Anhydrite laths in siltstone (3320–3350 ft). Vertical field of view is 3.2 mm.* ***(A&C)*** *are in plane-polarized light,* ***(B&D)*** *are in crossed-polarized light.*

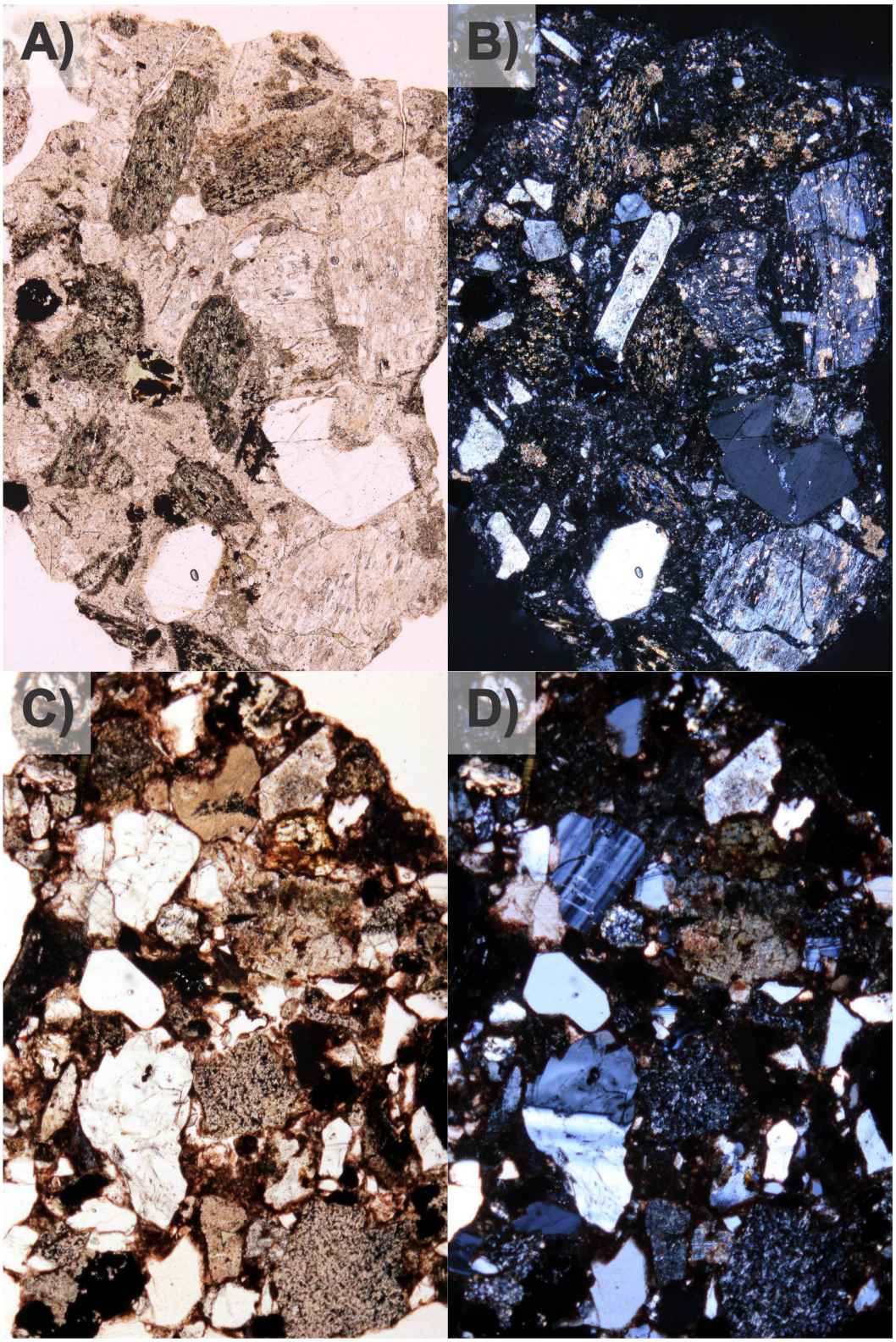

Figure B2. 4380–4400 to 5440–5450 ft: *Representative photomicrographs of alluvial deposits.* ***(A&B)*** *4840–4850 ft. Vertical field of view is 3.2 mm.* ***(C&D)*** *5240–5250 ft. Vertical field of view is 3.2 mm.* ***(A&C)*** *are in plane-polarized light,* ***(B&D)*** *are in crossed-polarized light.*

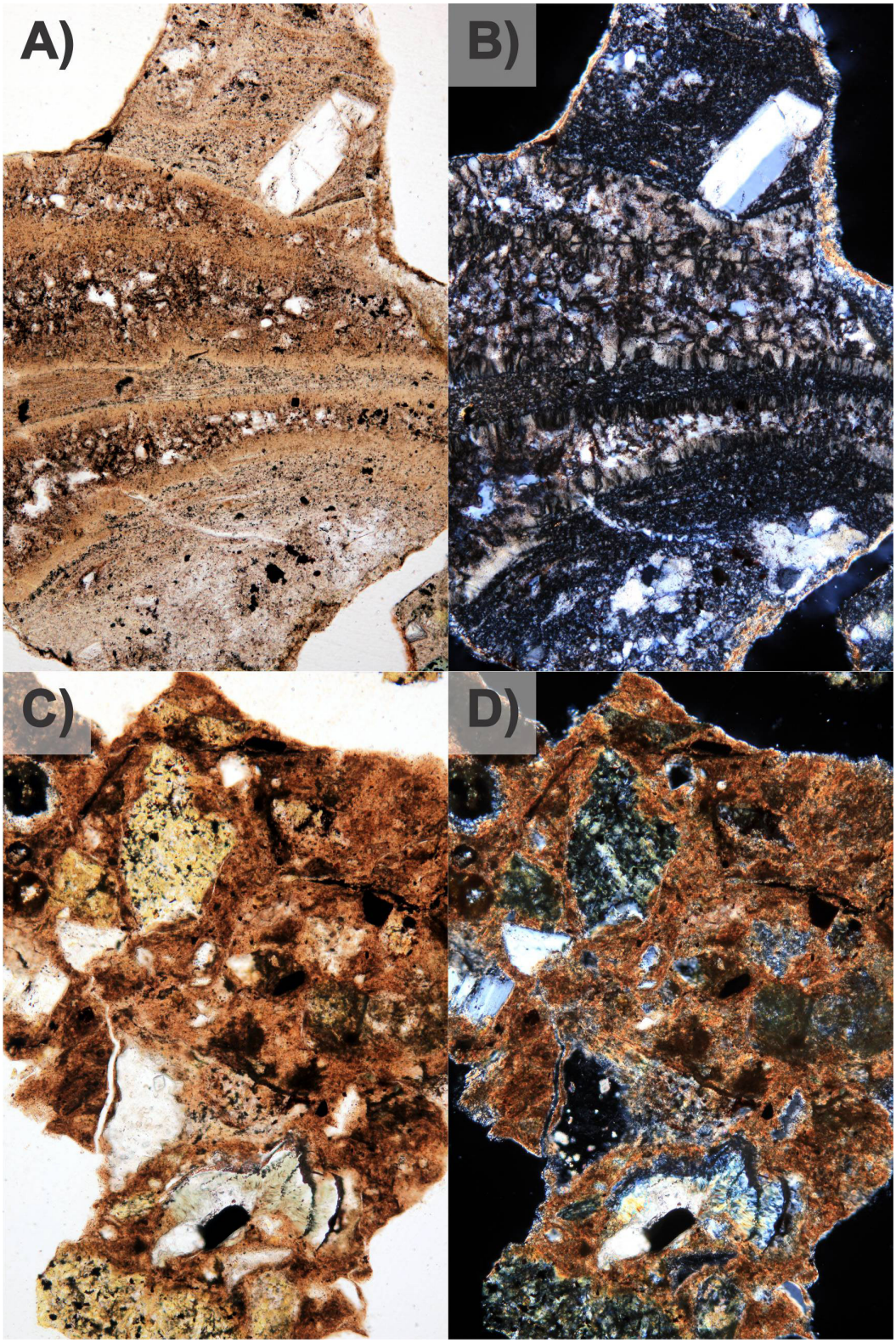

Figure B3. 5640–5650 to 6990–7000 ft: *Representative photomicrographs of rhyolite ash-flow tuff and tuffaceous sediments.* ***(A&B)*** *Devitrified ash-flow tuff with a sanadine phenocryst (5840–5850 ft). Vertical field of view is 1.6 mm.* ***(C&D)*** *Tuffaceous sediment (6040–6050 ft). Vertical field of view is 1.6 mm.* ***(A&C)*** *are in plane-polarized light,* ***(B&D)*** *are in crossed-polarized light.*

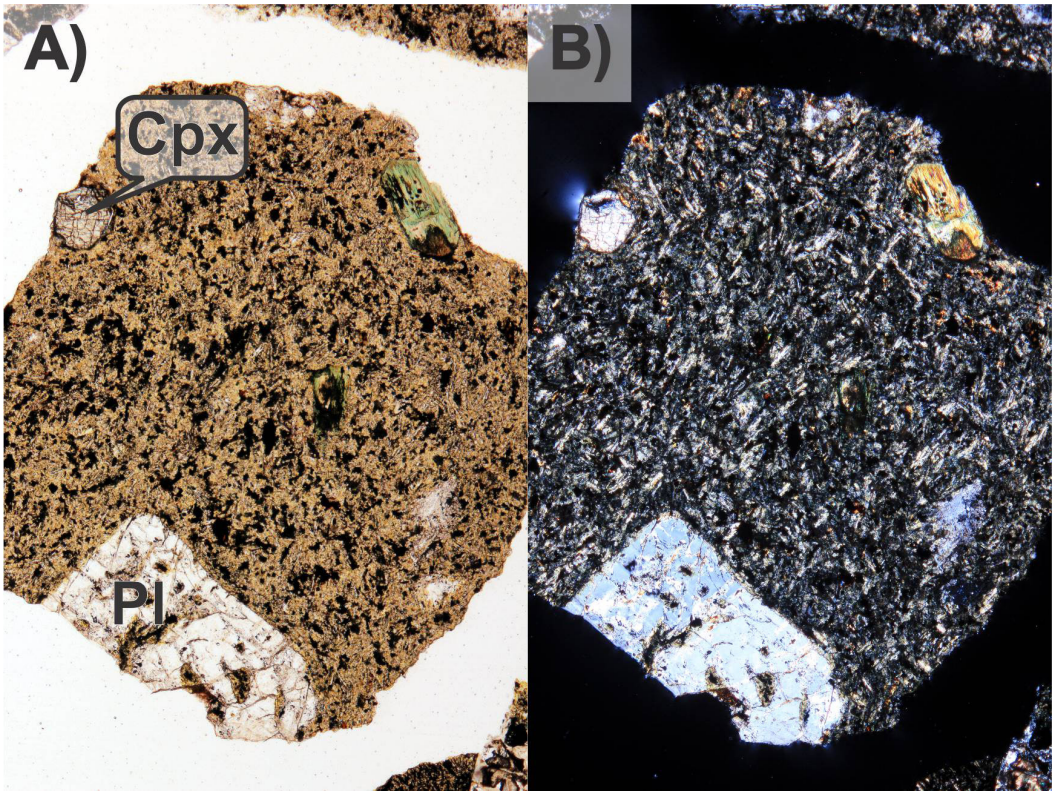

Figure B4. 7220–7250 to 7540–7550 ft: *Andesite flow with plagioclase (Pl) and clinopyroxene (Cpx) phenocrysts in a fine-grained groundmass (7540–7550 ft). Vertical field of view is 3.2 mm.* ***(A)*** *is in plane-polarized light,* ***(B)*** *is in crossed-polarized light.*

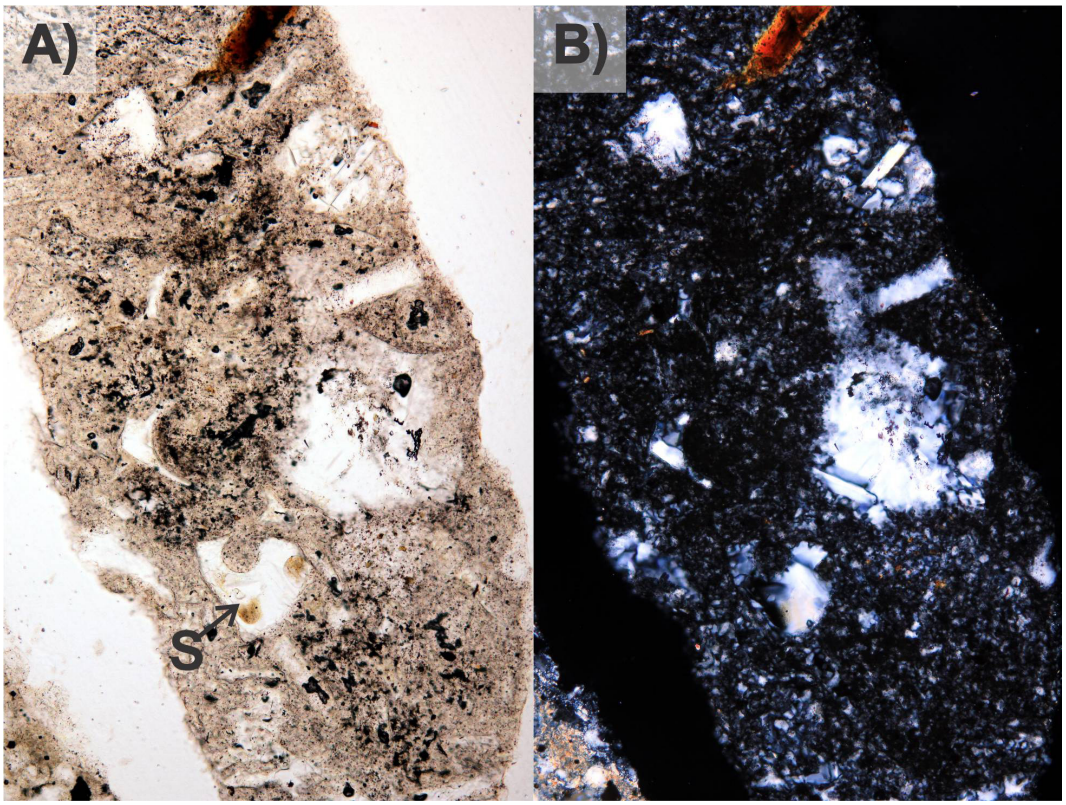

Figure B5. 7740–7750 ft: *Rhyolite ash-flow tuff devitrified shards (S) in a fine-grained matrix. Vertical field of view is 1.6 mm.* ***(A)*** *is in plane-polarized light,* ***(B)*** *is in crossed-polarized light.*

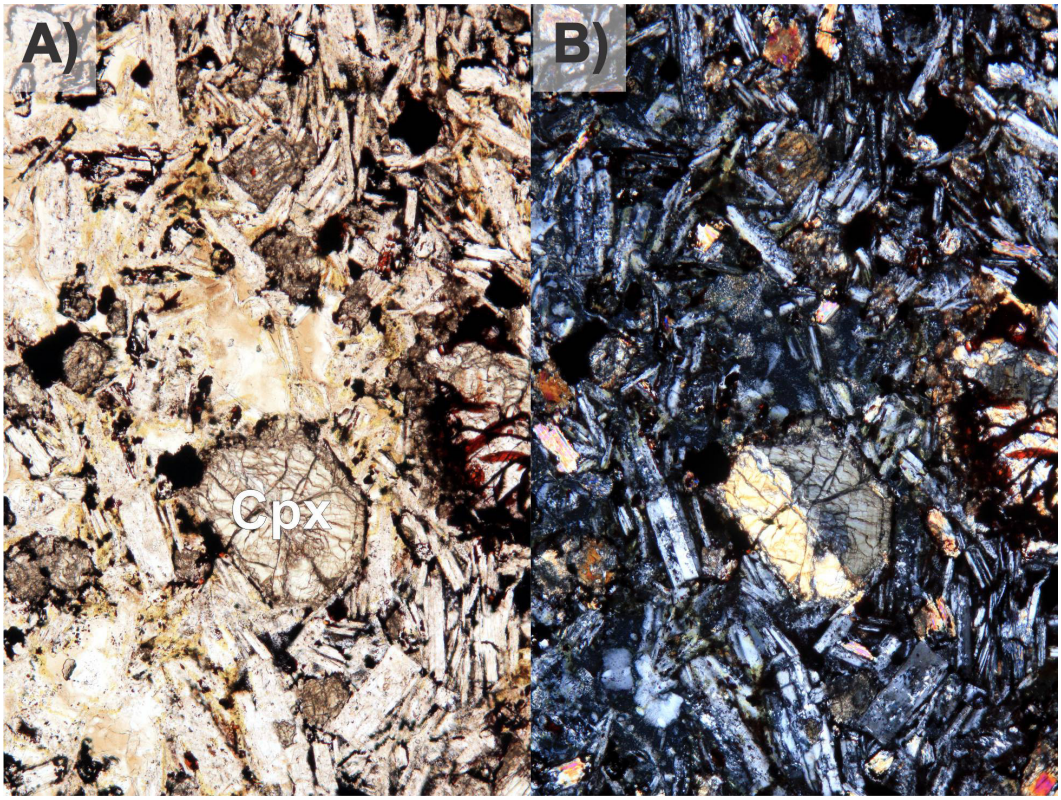

Figure B6. 7990–8000 ft: *Andesite flow with a clinopyroxene (Cpx) phenocryst in a groundmass of plagioclase laths. Vertical field of view is 1.6 mm.* ***(A)*** *is in plane-polarized light,* ***(B)*** *is in crossed-polarized light.*

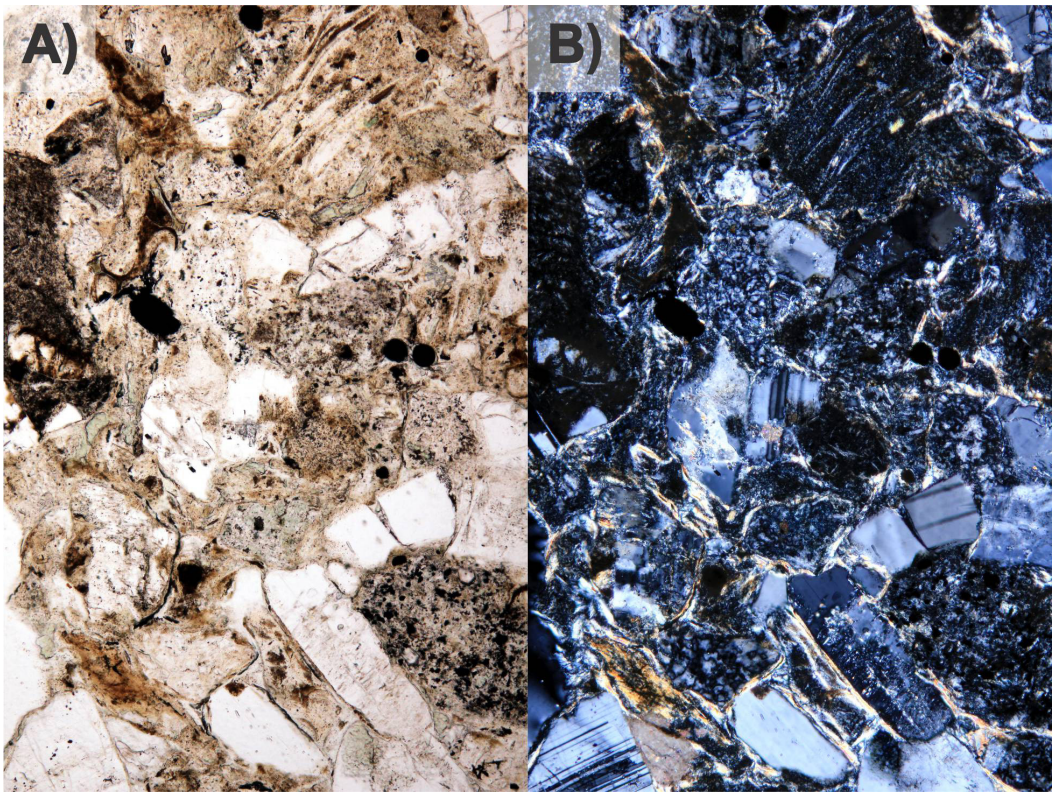

Figure B7. 8240–8250 to 8740–8750 ft: *Representative photomicrographs of volcaniclastic sandstone (8740–8750 ft). Vertical field of view is 1.6 mm.* ***(A)*** *is in plane-polarized light,* ***(B)*** *is in crossed-polarized light.*

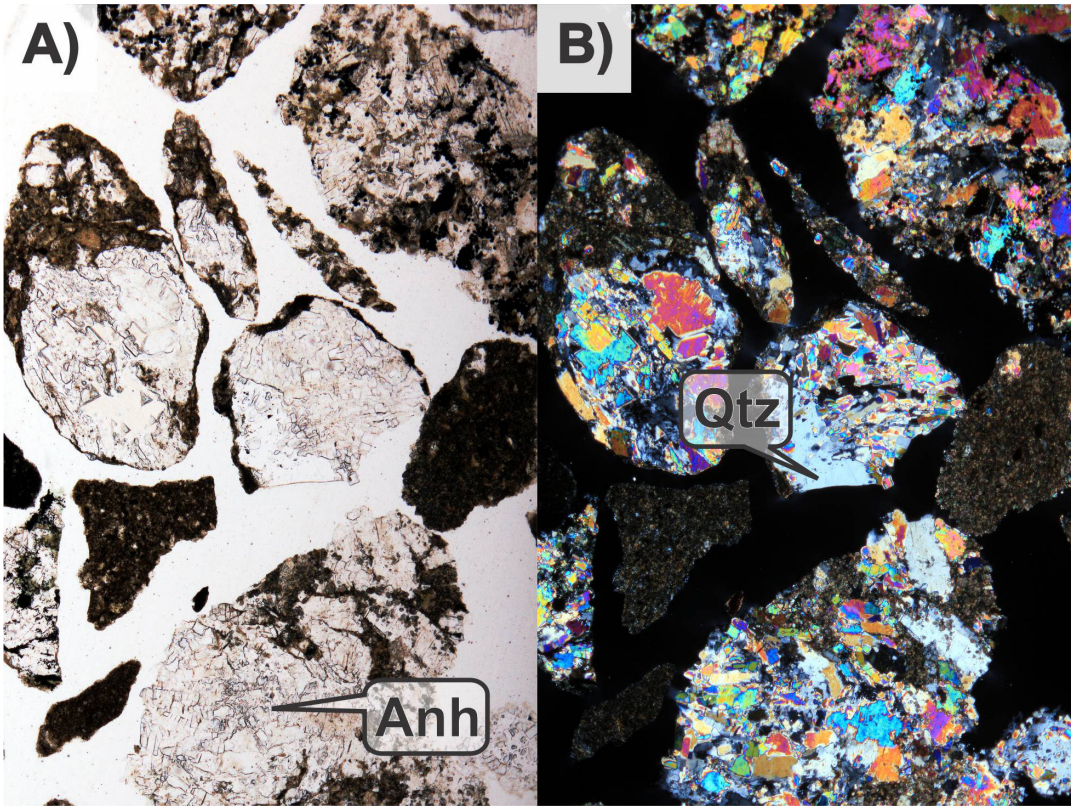

Figure B8. 8940–8950 to 9340–9350 ft: *Anhydrite nodules in siltstone 9340–9350 ft. This lithologic unit is composed of lacustrine and evaporite deposits. Vertical field of view is 3.2 mm.* ***(A)*** *is in plane-polarized light,* ***(B)*** *is in crossed-polarized light.*

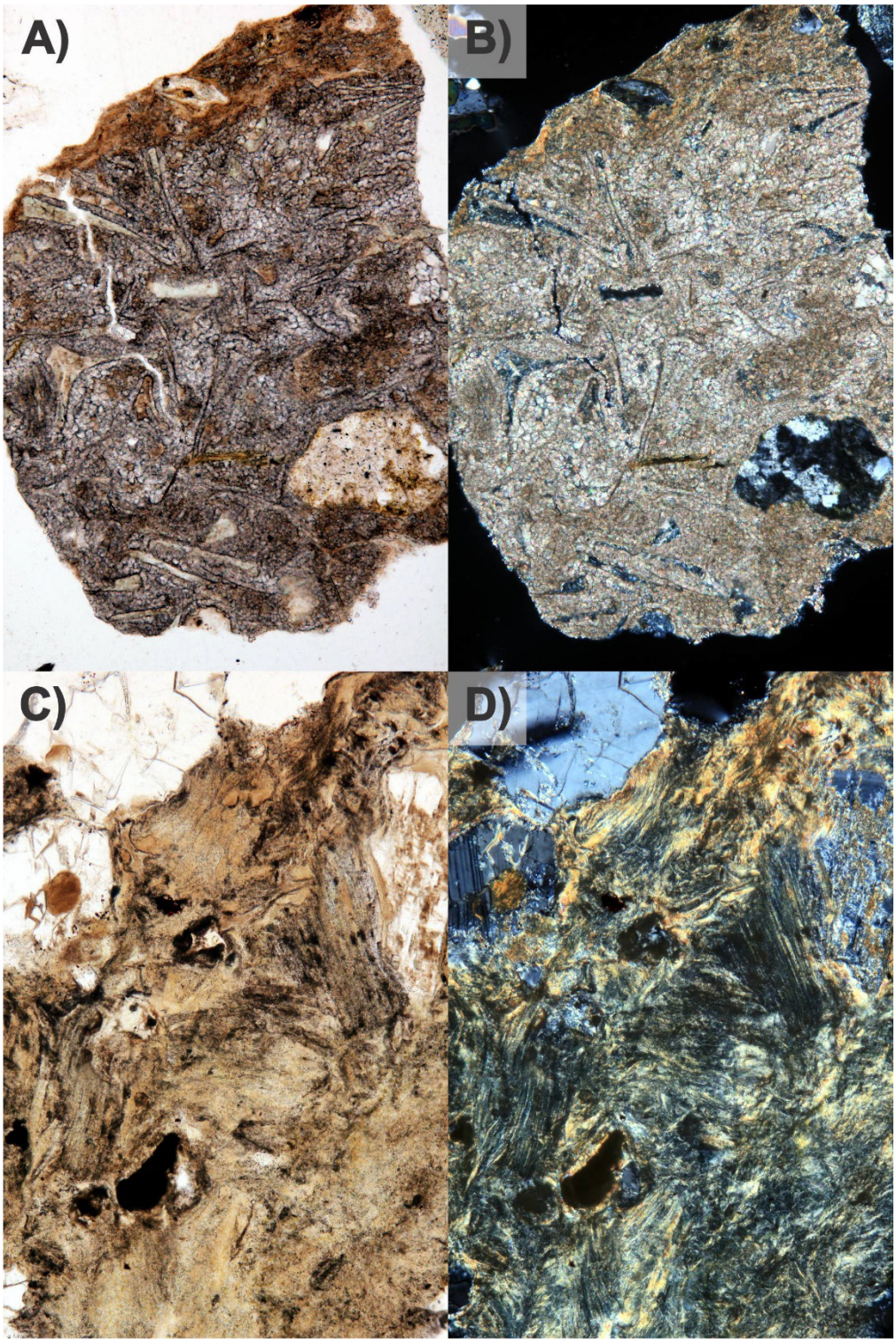

Figure B9. 9540–9550 to 10140–10150 ft: *Representative photomicrographs of rhyolite ash-flow tuff. This lithologic unit also contains tuffaceous sediments.* ***(A&B)*** *Shards in a carbonate matrix. Images of sample 9540–9550 ft. Vertical field of view is 3.2 mm.* ***(C&D)*** *Pumice (fiamme) textures in an ash-flow tuff. Images of sample 9940–9950 ft. Vertical field of view is 1.6 mm.* ***(A&C)*** *are in plane-polarized light,* ***(B&D)*** *are in crossed-polarized light.*